LA ROCHELLE UNIVERSITÉ
FACULTÉ DE SCIENCES ET TECHNIQUES
MASTER 2 SPE– Géophysique et Géosciences du Littoral 2022-2023

Sensor Inter-Comparison Analysis At Saint-Paul Island

Florence HENRY

Internship from February 2023 to June 2023 at LIENSs Laboratory Scientific Supervisor: Laurent Testut (Researcher)

Table of Content

Acknowledgements

First of all, I would like to thank Laurent Testut for giving me the opportunity of this internship with LIENSs and CNRS, for his availability and kindness. I am grateful to Philippe Téchiné from LEGOS for his reactivity to provide me data, to Victor from LIENSs for the latest Saint-Paul station memory data that he collected mid-April 2023 on site, and which have improved significantly the results.
I thank my office mates: Nushrat, Tanguy, Louise, Wassim and Léo, who made a pleasant atmosphere in the office to work and talk about sciences and as well as all other persons who helped me during this internship.

Executive Summary

The Saint-Paul Island sea level station, located in the southern part of the Indian Ocean, has been enriched the past decade with open-air radar gauge and permanent GNSS station in addition to the existing bottom pressure and radar gauges installed at a stilling tube. Calibrations and comparisons of the sea level data sets are essential to assess the quality of the data and to ensure their usefulness for applications like the mean sea level trend analysis in the context of climate change. A multi-comparison over the period 2018-2023 was performed to access the stability and performance of the tide gauges, identify errors, estimate their magnitude and to set-up a reference sensor for Saint-Paul Island site. The results showed the superiority of the open-air radar sensor in terms of stability, especially for remote site with maintenance limited in duration like in Saint-Paul while the bottom pressure and radar gauges at the stilling tube are subject to bias (drift, scale factor…). In addition, the ability of the GNSS reflectometry approach to monitor the sea level variations was checked and could be a promising alternative way to tide gauge for sea level trend analysis. The study also evidenced that having several tide gauges operating simultaneously and different storing -transmission support is worthwhile, especially for remote site like Saint-Paul Island.

1 Introduction and Objectives

Sea level measurement has been for long time an important component of many onshore and offshore services such as defining the hydrographic zero, monitoring (or analysing) ocean tide, facilitating harbour operations and aiding navigation. However, with the global climate change and its direct societal impact for coastline communities, the monitoring of the sea level is fundamental for understanding the variability of ocean dynamics at different time scales and becomes a key climate change index (Douglas, 2001; Holgate et al. ,2013; Woodworth et al.,2003; Church and White,2006). However, many tide gauges, which are suitable for harbour operations, are not accurate enough for long-term sea level studies. Therefore, significant efforts are being made worldwide to increase the tide gauge networks and upgrade them using new technologies. The performance of tide gauges has been given considerable interest over the past decades, in particular in the context of the Global Sea Level Observing System (GLOSS) programme (IOC, 2006; Woodworth et al.,2003; Merrifield et al. 2010; Miguez et al., 2005, 2008, 2012; Perez et al., 2013; Testut et al.,2006, 2010).
The ROSAME network, part of the GLOSS network, sets up modern tide stations in the Terres Australes et Antarctiques Françaises (TAAF) in order to densify sea level observations in the southern Indian Ocean and to respond to scientific attention regarding the global sea level rise and the studies of ocean and climate dynamics in this region (Figure 1). The district of Saint-Paul and Amsterdam Islands, is located at the southwestern end of the Australian plate, approximately 1,325 km north-northeast of the Kerguelen Islands. They represent one of the few emergent points of a large submarine volcanic plateau along the Southeast Indian Ridge (https://www.amaepf.fr/).

Saint-Paul Island (38°41'S, 77°31'E) is an ancient volcanic island, which collapsed some thousand years ago and got inundated (Figure 1). Saint-Paul island has a mild oceanic climate influenced by the convergence zone of subtropical and sub-Antarctic waters at about 500 km further south and by the westerlies, known as the roaring forties. The sea surface temperature varies from approximately 12°C in August to 18°C in February.

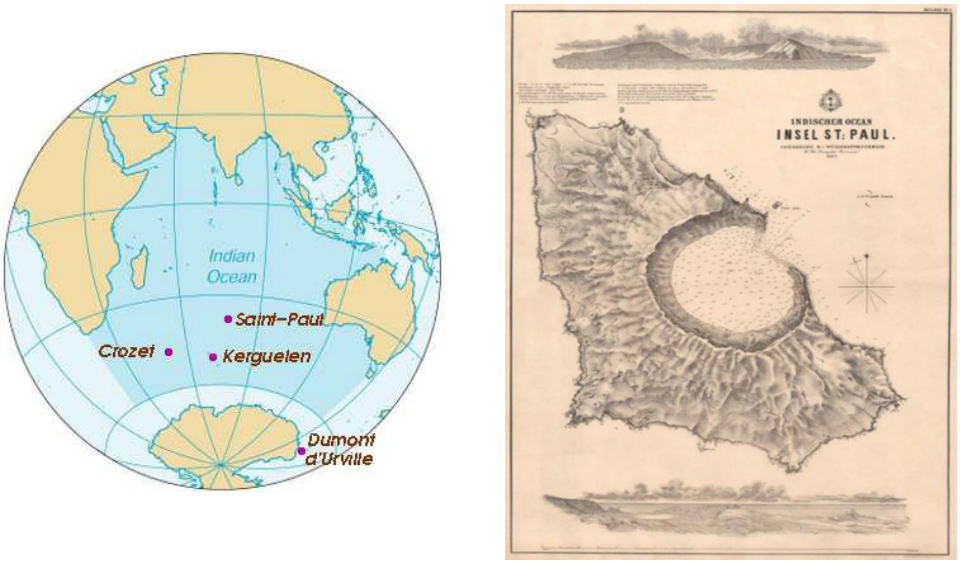

Figure 1 : Location map of Saint-Paul Island (LEGOS) and Saint-Paul Island sketch issued from "Novara" scientific expedition in 1857 showing the island geomorphology

Discovered in sixteen century and then site for scientific expeditions, a historical mean sea level was defined in 1874 and confirmed as a mean sea level reference point after archaeological and scientific investigation between 1994 and 2006 (Testut et al.,2010). Saint-Paul Island and its remote location in the Southern part of the Indian ocean, represents a site of particular interest of sea level studies. Indeed,

the availability of the sea level time-series is mostly restricted to continental coastlines and information about the variability of ocean dynamics for different time scales, especially in open ocean for the Southern Hemisphere, are limited.

Since October 1994, Saint-Paul Island hosts an automatic sea level observatory, which is located within the ancient crater (Figure 2) playing the role of natural stilling well. This sea level has consisted in early stage of a bottom pressure tide gauge installed in a stilling tube and a satellite data transmission system, which get completed with two radar tide gauges (one installed at the upper plate of the stilling tube in 2007 and one in open-air in 2018), a permanent GNSS station in 2011 and few temporary GNSS buoy sessions. Testut et al. (2010) made an estimate of the mean sea level rate for the period 1874-2010 and the associated errors for the historic and modern periods and instruments. The inter-comparison of the sensors on site was limited since the radar tide gauge broke down 7 months after its installation in 2007; the spatial altimetry was used to calibrate the bottom pressure gauge prone to drift. Since then the Saint-Paul sea level observatory has got upgraded with an open-air radar gauge and GNSS reflectometry approach is applied to retrieve sea level measurement from GNSS data. The period 2018-offers the longest time window, during which the sensors work simultaneously.
The objectives of this study for Saint-Paul Island site are firstly, to have clear overview of the database over the period 1994-2023. The database has become complex with time because of the multi-supports and formats for storing and transmitting sea level data. Secondly, the multi-comparison has to enabled us to evaluate the stability and performance of the different gauges, identify errors, estimate their magnitude and to set-up a reference gauge for Saint-Paul Island site. The instrument error can be then estimated at Saint-Paul remote observatory. In addition, the comparison of the radar gauge installation: stilling well versus open-air context can provide the opportunity to investigate the effect of the stilling tube on the sea level measured by a same technology. Finally, the ability of the GNSS reflectometry approach to monitor the sea level variations will be investigated as well in this study.

In this report, after providing an history of the evolution of Saint-Paul observatory in section 2, some considerations are made regarding the functioning of the tide gauges and data processing in section 3. The inter-comparison of the sea level data is performed in Section 4 over the most recent period (2018 – 2022) in order to identify the potential uncertainties and estimate their magnitude. Finally, section 5 contains the discussion and conclusions of the study.

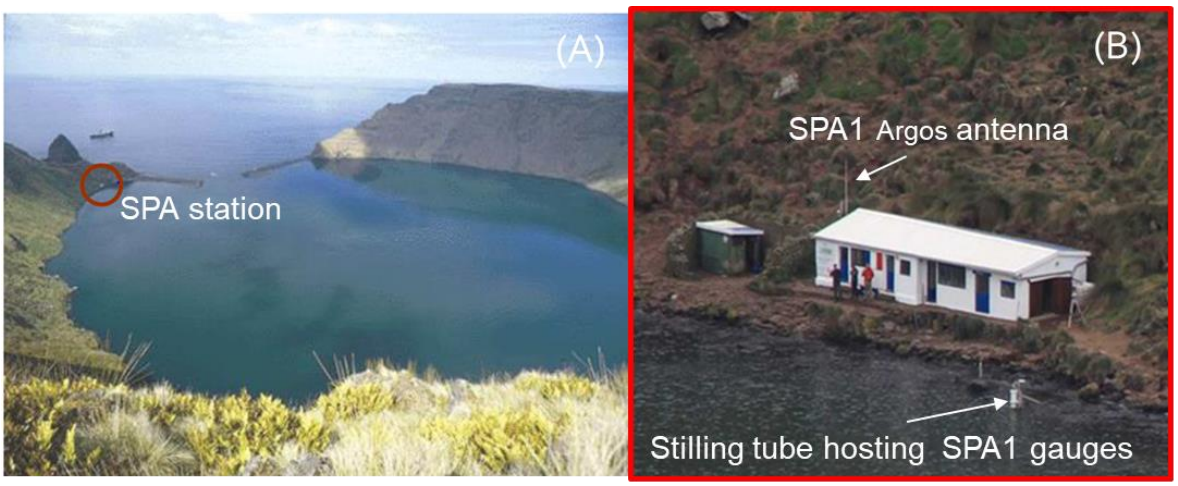

Figure 2 : (A) Location map of Saint-Paul Island sea level observatory (LEGOS), (B) Photo of Saint-Paul Island Sea Level observatory in 2014 (Adapted from Nivmer report)

2 Chronology of Saint-Paul Island Sea Level Observatory

2.1 Historical measurements

In September 1874, Saint-Paul Island was the destination of a scientific expedition directed by Amiral Mouchez for the observation of the Venus transit in front of the Sun. It is during this expedition that the first sea level measurements in Saint-Paul Island were continuously recorded with a help of a tide pole every half an hour from 6 October 1874 to 31 December 1874 (Testut et al., 2010). The mean value of these measurements (uncorrected for the inverse barometer effect) was calculated in-situ and then transferred to a mark struck in a rock (Figure 3). Meteorological parameters such as atmospheric pressure, humidity and air temperature were as well recorded during this expedition. The rock mark, rediscovered in 1994 during an archeological inventory, was attributed to the mean sea level reported by Amiral Mouchez memories in 1878. It was confirmed as reference point to establish the evolution of Mean Sea Level (MSL) at the island after a quality assessment of the sea level observations; the total error relative to the 1874-MSL mark was estimated to 5.8 cm (Testut et al., 2010). This historical mean sea level mark was then levelled during NIVMER maintenance missions in 2006, 2007, 2008 and 2010.

Figure 3 : Saint-Paul Island 1874 mean sea level mark (Testut et al.,2010)

2.2 Modern measurements

The Saint Paul Island station, established in October 1994, is automatic and evolutive since then. The human maintenance in Saint-Paul island site is limited in duration since Saint-Paul Island is classified as Natural Reserve and long period of human presence is not allowed. The remote location does not allow rapid action in case of technical problem of the tide gauge station. The maintenance frequency is mainly on yearly basis during the logistical rotation of the French research vessel Marion Dufresne. A history of the NIVMER maintenance missions on site is available from ROSAME website. No tide pole was set-up in Saint-Paul since the island is inhabited.

Figure 4 summarizes the operational periods of the different permanent sensors (SPA_BARO: Barometric sensor; SPA2_RDR: SPA2 open-air radar gauge; SPA1_RDR: wave-guided radar gauge, SPA1_BPR: Bottom pressure gauge and GNSS permanent stations use for Vertical Land Motion (VLM) estimation or reflectometry GNSS-IR approach, the complementary campaigns of measurements performed during the mission on site (optical probe calibration, static GNSS recording, GNSS buoy recording and levelling), and the main maintenance operation on sensors .

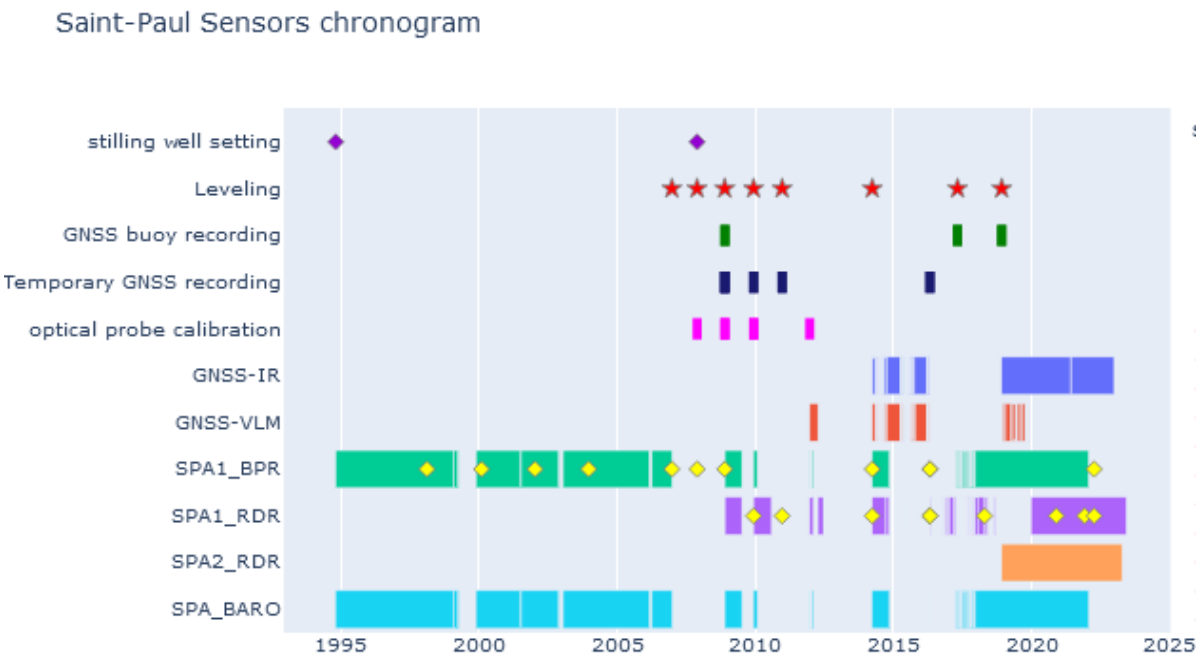

Figure 4 : Chronogram of Saint-Paul Island sensor operational periods (SPA_BARO: Barometric sensor; SPA2_RDR: SPA2 radar tide gauge; SPA1_RDR: wave-guided radar tide gauge, SPA1_BPR: Bottom pressure tide gauge and GNSS-VLM: GNSS derived vertical land movement and GNSS-IR: GNSS reflectometry), temporary measurements campaigns and major maintenance operation on sensors (yellow diamonds)

- SPA1 station

The first modern tide gauge station installed at Saint Paul Island was equipped with an Aanderaa WLR7 bottom pressure gauge installed in a stilling well. The pressure tide gauge measures changes in the bottom pressure (including the sea water level column and atmosphere) and are equipped with a temperature sensor and a conductivity sensor (since 2003). In addition, a barometric sensor is installed in the station cabin. The sea level measurement is derived from the difference between bottom and atmospheric pressure considering the value of local gravity and the sea water density. Density is derived from in situ ocean temperature and salinity. The accuracy of pressure tide gauge is sub-centimetric (5 mm < σ < 1 cm). Measurements began on 25 October 1994 and are transmitted by ARGOS telemetry to LEGOS in Toulouse. From October 1994 to November 2007, the measurements are continuous with a few short gaps due to station battery failure or data transmission problems. In November 2007, the stilling tube is changed and an ARGOS-DT insu (real time developed by CNRS) station is set-up. From November 2007 to 2017, long gaps of measurements occur because of station power supply issues and serious electronic connection failure between the sensor and the station; during that period, the pressure tide gauge has been set-up to work in autonomous mode on temporally basis. From Dec 2017 (new station power supply) to April 2022, the measurements are continuous. Since April 2022, the pressure tide gauge is not operational; a diagnosis to detect tide gauge physical or connection problems is still running on during the short-time maintenance visit. It is important to notice that the pressure tide gauge is removed on yearly basis from the stilling tube to be cleaned from strong concretions or to be changed for a new calibrated pressure tide gauge. No levelling operation is done on routinely basis before and after each change of the pressure tide gauge because of campaign limited time.

Since November 2008, the SPA1 station has been equipped with a wave-guided radar gauge (SPA1_RDR) (Khrone Optiflex 1300C) installed at the top of the pressure tide gauge stilling tube. The SPA1 radar sensor detects microwave pulses that are reflected by the air/sea interface, by measuring the transit time of the signal. The wave-guided radar tide gauge is synchronized on the GPS clock as the pressure tide gauge; the ARGOS antenna transmits the data for both sensors. Unfortunately, from November 2008 to early 2020, the measurement recovered are on episodic basis because of an electronic failure

of the station, implying a large loss of data. The radar tide gauge was changed in 2014 for a stainless version of the Khrone Optiflex 1300C.

- Complementary observations

Sea level measured by a tide gauge is a sea level height relative to the level of benchmarks on the nearby land, so vertical motion of land will cause an apparent sea-level change. Thus, in parallel to tide gauge sea level data, from 2006 campaigns of measurements were carried to control tide gauge datum and vertical land movement in Saint-Paul, and consist of:

- Regular optical levelling surveys conducted between 2006 and 2011 and then between 2014 and 2018. The optical levelling is used to establish the relative heights levels of tide or geodetic benchmarks relative to the Saint-Paul hydrographic zero (Zh_LEGOS). The levelling measurement is local, punctual, and one-dimensional. The expected resolution is between 1/10 mm and 1 mm.
- Static global navigation satellite system (GNSS) campaigns were undertaken in 2008, 2009, 2010 and 2014. This technology uses signals from satellites to pinpoint a location on the Earth's surface. In addition to transmitting information about location, GNSS provide locally a 3-D displacement vector of the permanent station. The GPS measurement has a resolution of few mm.
- GNSS equipped buoy sessions deployed close to the stilling tube (Figure 5) during 2-days NIVMER missions in 2008, 2016 and 2018. The instrument used was a GNSS Trimble associated a TOPCON GB1000 antenna as receiver installed on geodetic benchmark. GNSS techniques have been successfully used to perform in-situ calibration of tide gauges in remote islands (Watson et al.,2008, Testut et al. 2010, Miguez et al.,2012) and define the absolute datum of the tide gauges. GNSS buoy is an effective technique for measuring coastal sea level independently from land level at 1-5 mm-accuracy (Andre et al., 2013)
- Optical probe reading in 2008 and 2011 done to calibrate SPA1 radar tide gauge (SPA1_RDR).

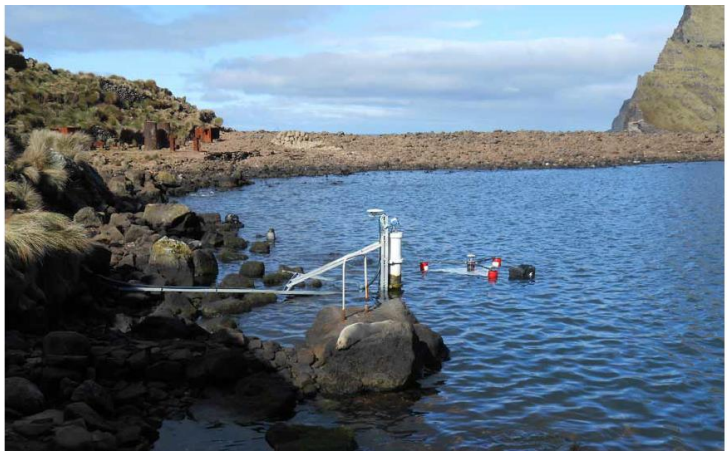

Figure 5 : GNSS buoy measurement session in April 2016 (NIVMER report)

In December 2011, a permanent GNSS antenna was set-up on top of the stilling tube structure associated with a GNSS Trimble NETR9 receiver installed in the cabin (Figure 6). The receiver (Trimble NetR9) and antenna can track multiple GNSS constellation signals: GPS, Galileo, GLONASS and provide a permanent monitoring of the vertical and radial movements referenced into a well-defined terrestrial reference frame. The GNSS antenna position was modified in November 2018 and has been moved up to a triangular support on the SPA2 arm structure.

In parallel to the geodetic positioning, GNSS Reflectometry approach is applied to retrieve the sea level height from GNSS data from 2014. The GNSS reflections off the sea surface, normally a source of error and noise in geodetic positioning processing, generate characteristic oscillations in received signal strength; an analysis of the signal to noise ratio of these variations is use to estimate the height of the

reflected surface (Larson et al. 2013; Löfgren et al. 2014, Larson et al. 2017; William et al., 2020) with a general accuracy of 2 cm for daily mean.

- SPA2 station

From November 2018 onwards, the sea level observatory hosts a microwave radar gauge: Krohne Optiwave 7300C (SPA2_RDR), which is installed in open-air condition at less than 1-meter from SPA1_RDR and SPA1_BPR (Figure 7). Its associated SPA2 station is installed in the nearby cabin and includes its own ARGOS transmission system (Figure 7). The SPA2 radar tide gauge is operational continuously since November 2018. The accuracy of the radar gauge is sub-centimetre (1 mm < σ < 5 mm).
All the sensors are synchronized on the GNSS time through a GNSS chip.

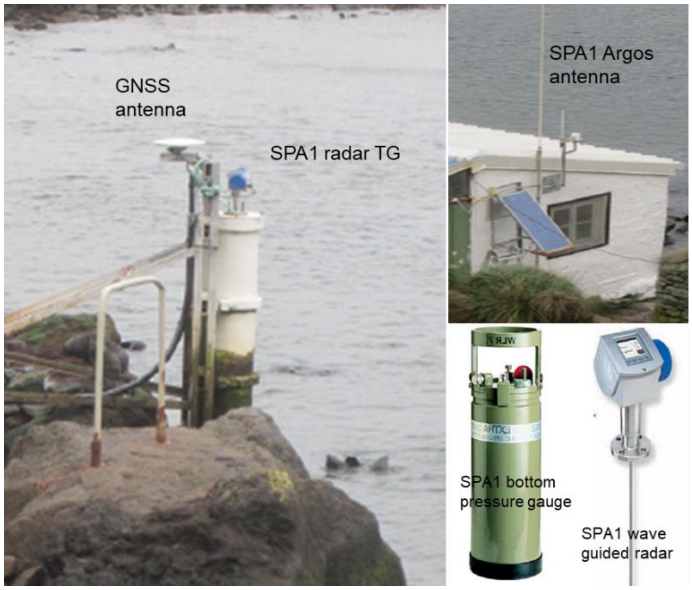

Figure 6 : Saint-Paul SPA1 station in 2014 with the stilling tube hosting the bottom pressure gauge (SPA_BPR), the wave guided radar gauge (SPA1_RDR) and the GNSS antenna; ARGOS antenna is set-up on the side of the cabin (Adapted from Nivmer report photos)

Figure 7 : Saint-Paul SPA1 and SPA2 stations in November 2018 upgraded with an open -air radar gauge (SPA2_RDR); SPA2 radar data are transmitted independently from SPA1 data by using two stations and ARGOS antennas (Adapted from Nivmer report photos)

3 Data Collection, Quality and Treatment

3.1 Data storage and transmission

Different supports and data formats have been used in Saint-Paul Island to store and transmit the sensor data, which make the database rather complex. The main data transmission system relies on an ARGOS antenna, which was set-up in early stage on the tide station installation. Real-time data are available from LEGOS-ROSAME ftp site with a sampling rate of 1-hour for SPA-1 radar sensor (SPA1_RDR) sharing the transmission line with the pressure tide gauge and 20 mn for SPA-2 radar sensor. In parallel, "Argos" files treated and provided by LEGOS are delivered at one- hour sampling. In addition to this, tide gauge sensors sent their data directly to the station which stores internally the data from the different sensors with various time samplings: 3mn, 10 mn and 1 hour depending on the sensors. The station memory files are collected during the NIVMER missions. The time assigned to the data sensors are normally synchronised on the GNSS clock.
Figure 8 displays the radar tide gauge data file timeline with their respective sampling rate for the different received data flux (mdat_: DT-INSU station memory data; memodt_ and memo_: memory data, arg_: stored real-time data; rt_: real time data from ftp site).

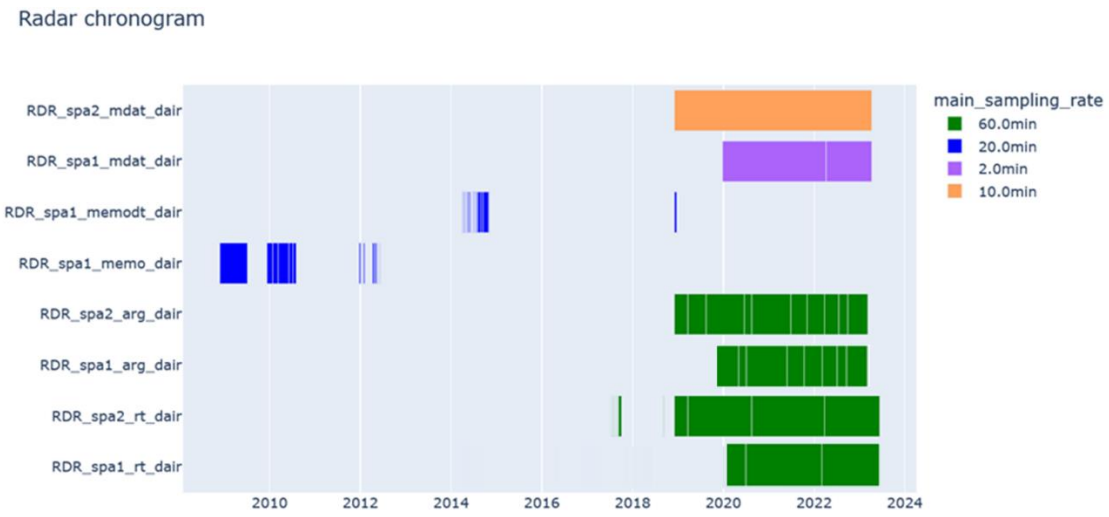

Figure 8 : Saint-Paul radar tide gauges timeline and their respective sampling rate (mdat_: DT-INSU station memory data; memodt_ and memo_: memory data, arg_: stored real-time data; rt_: real time data from ftp site)

3.2 Optical Levelling

A possible source of offsets between different records is related to the change and cleaning of the equipment during the maintenance campaign. Precise levelling with respect to a permanent benchmarks network must be undertaken in order to have the correct height of the gauge contact point and establish a common reference for the full record. In Saint-Paul Island, no hydrographic zero has been defined by SHOM (Service Hydrographique et Océanographique de la Marine). An arbitrary hydographic defined as Zh_LEGOS was set-up in Testut et al. (2010) as 4 m below geodetic benchmark D being the main marker sealed on the step-in front of the cabin. The benchmark D is used as the geodetic reference point and has been referred to terrestrial reference frame from GNSS campaign.
The levelling campaigns had been performed for different geodetic points on site and sensor contact points relative to the benchmark D. The localisations of the major benchmarks are provided in Appendix A -Figure A1. Figure 9 summarizes the levelling heights of the sensor contact points for the period 2018-2023; the description of the levelling is the followed:

- D: main marker sealed on the step-in front of the cabin,
- I: upper plate of the tide gauge tube serving as a support for the SPA1 radar sensor and its reference measurement point
- J: top of the metallic arm fixed to the stilling tube structure supporting the SPA2 radar gauge and used as its measurement reference point
- W: upper hand of the bottom pressure tide gauge
- C: intermediate marker sealed in the rocks at the pier
- U intermediate marker sealed on concrete of old building
- E: the historical 1874 mean sea level mark

The leveling height of the geodetic benchmarks in Figure 9 referred to the Nivmer levelling campaigns of 2007, 2008, 2009. One-centimetre discrepancy exists with the levelling campaign from Mission Patrimoine in 2O10 for the benchmarks C and E.

The sensor contact levelling heights are used to define the sea level measured by the different sensors relative to Zh_LEGOS. For the period anterior to 2018, the summary of the levelling campaign for the major change in the sensor contact point is provided in Appendix A.

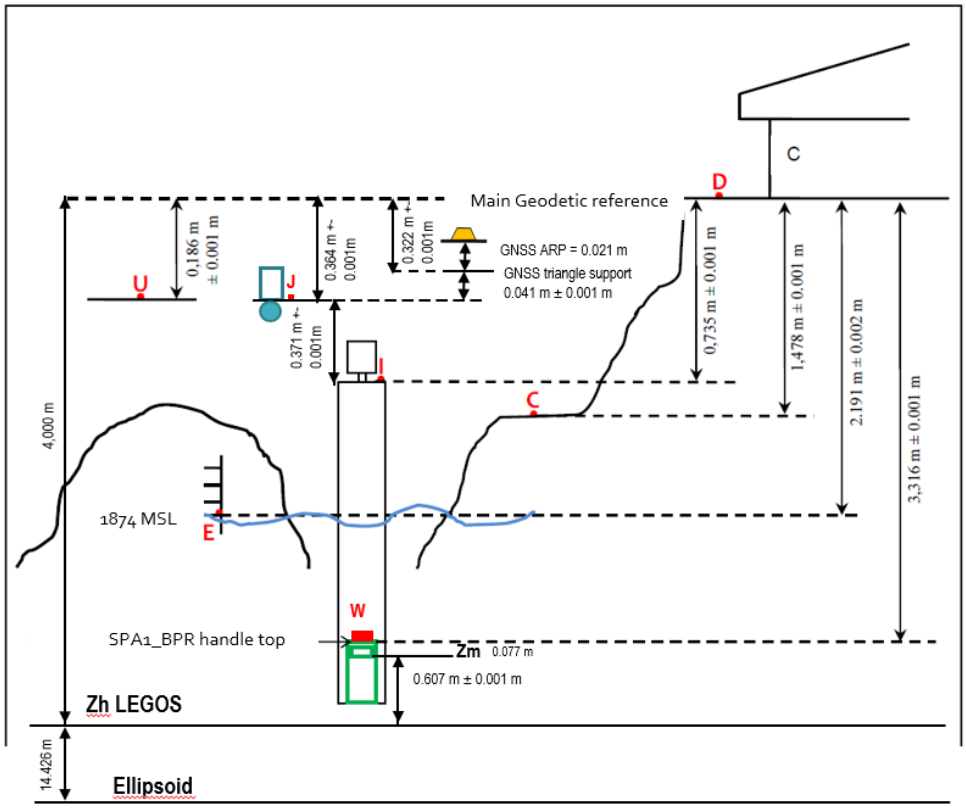

Figure 9 : Levelling summary for the period Dec.2018 – Mar. 2023 (Adapted from IGN and Nivmer reports)

It is important to notice that the levelling campaigns have been carried out mainly from 2006 to 2010 and in 2018, which implies that mean sea levels obtained prior to 2006 and post 2018 could be affected by errors associated with changes in the gauge contact point. This feature concerns the SPA1 radar tide gauge, which was removed for cleaning and stilling tube maintenance after 2018 and the SPA1 bottom pressure tide gauge for which the last levelling information is from 2010 while the gauge was replaced and cleaned several times since then. During the NIVMER operational visit in mid-April 2023, the available levelling data of this campaign are restricted to the levelling of the radar tide gauges contact points due to the limited time on site.

3.3 Sea Water Properties: Temperature, Salinity and Density

The sea water density enters in the equation for computing the sea level from bottom pressure measurement. The water density is derived from in situ ocean temperature which varies seasonally at Saint-Paul between 12 degC and 20 degC (Figure 8) and salinity. We have used the Python Seawater conversion package to compute water density. Although the salinity could be derived from the in-situ sea water conductivity measurements; these last ones being not reliable in case of Saint-Paul, the salinity was assumed to be constant and fixed to 33.9 psu (1psu = 1g/Kg) based on site information.

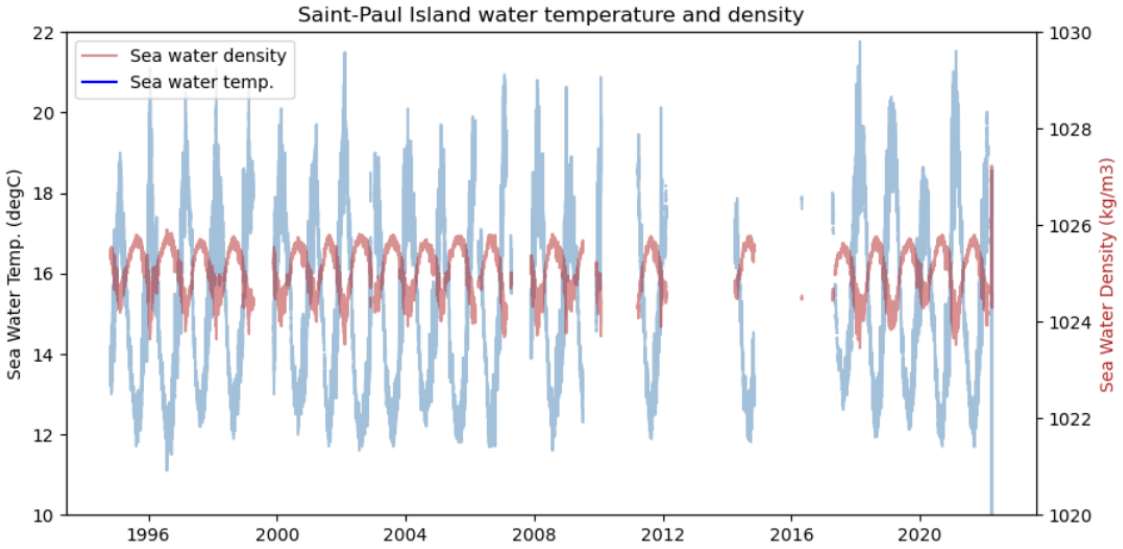

Figure 10 : Saint-Paul Island water temperature and density showing seasonal variation

3.4 Atmospheric Pressure Measurements

One of the causes of the sea level variability is due to meteorological forcing. Low pressure over the sea (depression) bulges the ocean surface whereas high pressure induces deepening of it. The influence of the weight of the air column above a given point on the ocean surface is calculated by the Inverse barometer. This associated sea level variation η_{ib} caused by the atmospheric pressure variation is defined by.

$$\eta_{ib} = -\frac{P_a - \overline{P_a}}{\rho . g}$$

η_{ib} : the sea level rise at a given point (m)
P_a : atmospheric pressure at this point (Pa)
$\overline{P_a}$: atmospheric pressure average over the ocean (Pa)
ρ : ocean water density (kg.m−3)
g : gravity acceleration (m.s−2) defined as function of the latitude and equals to 9.78 in Saint-Paul.

The atmospheric anomaly corresponding to the inverse barometer formula numerator is obtained by detrending the atmospheric pressure time series recorded by the station barometer using the linear least squares method.
Regarding the quality of the Saint-Paul atmospheric pressure itself between 1994 and 2007, the data presents an important drift between 1994 and 2007 as illustrated in Figure 11.

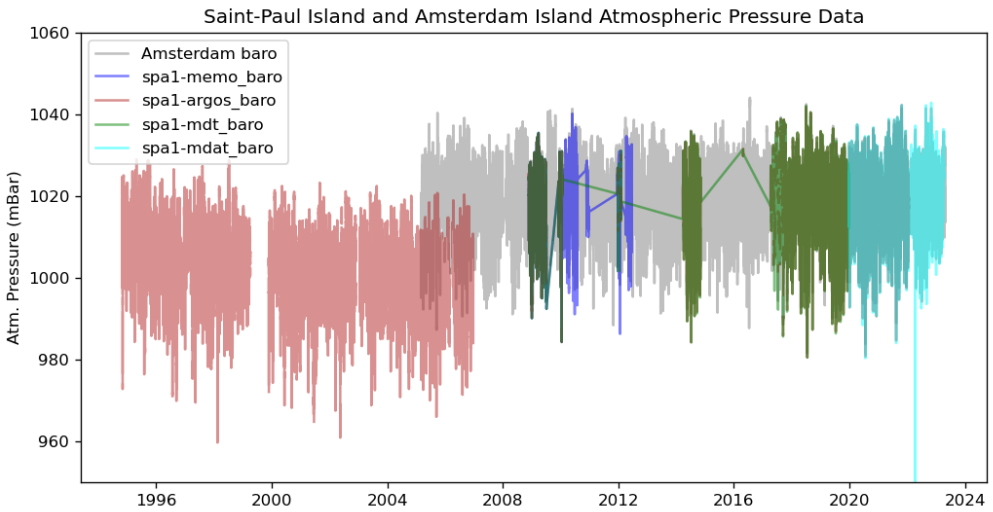

Figure 11 : Saint-Paul and Amsterdam Islands atmospheric pressure time series

Over the period 1994-2006, Testut et al. (2010) estimated a linear drift of 1 mbar/year after comparing Saint-Paul barometric data with atmospheric data recorded at the closest meteorological station of Amsterdam Island (located at 100 km up north). In the present study, the verification of the data with Amsterdam Island meteorological station could be done for the period of 2006 -2021. The barometric drift between Saint-Paul Island data and Amsterdam meteorological station is calculated from a linear least squares slope of the time series difference. Table1 provides the estimated barometric drift between both sites for the different sets of data. Apart from the period 2005-2007, the barometric drift between both sites is not significative. A drift correction will be only applied to the barometric data for the period 1994-2007 by detrending the data using a linear least square fit.

*Table 1: Saint Paul Island barometric drift estimate by comparison with Amsterdam Island meteorological station; *meteorological station data only available for the overlapping period 2005-2007.*

Period	Data source	Barometric Drift (mBar/y) by Meteo Stat. comparison
2005 - 2007	SPA1 Argos	- 0.473± 0.067*
2014 - 2023	SPA1 Argos	0.093 ± 0.012
2008 - 2012	Station memory	0.079± 0.042
2014 - 2019	Station memory	0.096± 0.008
2019 - 2023	Station memory	-0.037± 0.034

3.5 Sea Level Measurements

3.5.1 Radar gauge data

Radars are devices that measure the time taken by the emitted wave to travel the distance between the sensor and the surface of the water. This time is then converted into a distance that corresponds to the air draft between the device and the surface of the water. To obtain the sea level signal, it is therefore necessary to subtract from the signal the distance between transmitter/sensor and zero reference Zh_LEGOS

$$\eta_{Zh\_RDR} = RDR_{Zh} - Dair_{RDR}$$

where RDR_{Zh} is 3.265± 0.001 m for SPA1_RDR gauge and 3.636 ± 0.001 m for SPA2_RDR gauge. The contact point for the SPA1_RDR and SPA2_RDR tide gauges, as the reference point of their respective air draft measurement, is the base of the radar gauge flange.

- SPA1 radar gauge (SPA1_RDR) Data Quality Check

A preliminary quality check of the SPA1 radar air draft measurements from the different data storing support allowed the detection of suspicious behaviours. The SPA1 wave guided tide gauge was not operational from December 23rd, 2018 and January 4th, 2020. In 2020, the SPA1 radar gauge record shows a truncated signal at low tide over a long period spanning from January 1st, 2020 to November 23st, 2020 as illustrated in Figure 12 and occasionally during April-May 2021. The SPA1 wave guided radar located on the upper plate of the stilling tube seems to suffer from a stilling tube obstruction. This aspect has been confirmed by the NIVMER mission in December 2020 during which, the operational team need to detangle the bottom pressure tide gauge rod in the stilling tube.
In order to be able to use the high tide signal over this period in the subsequent, a data cleaning was performed to replace the plateau values at low tide by NAN value in optimal way. The retained method is based on the threshold criteria regarding the provided standard deviation σ of the air draft data and discard data according: $\sigma < 2$ mm and $\sigma > 100$ mm based on histogram analysis.

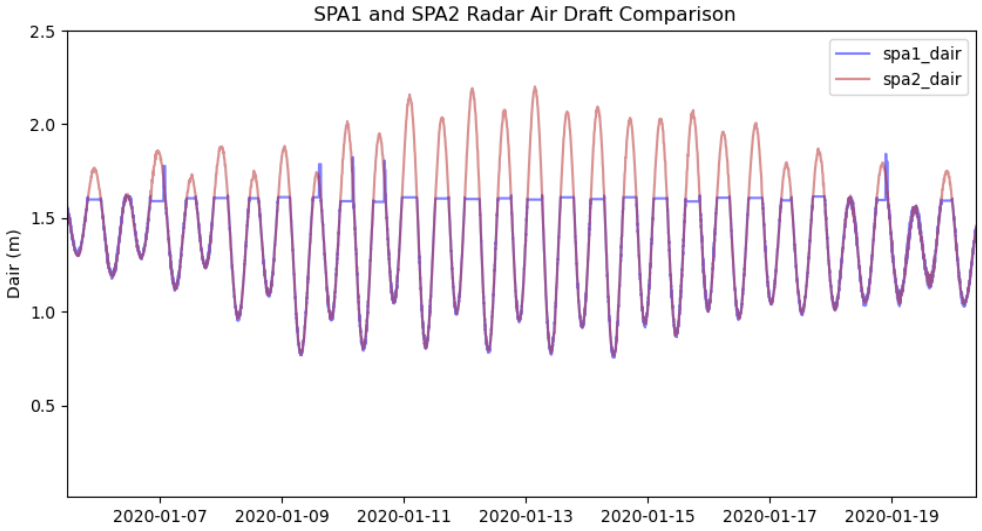

Figure 12 : SPA1_RDR truncated signal example occurring during 2020

During 2021, SPA1 and SPA2 radar sensors measure slightly different tide amplitude as shown in Figure 13. This issue will be analysed and quantified during the inter-comparison analysis to identify the sensor with a potential scale factor error.

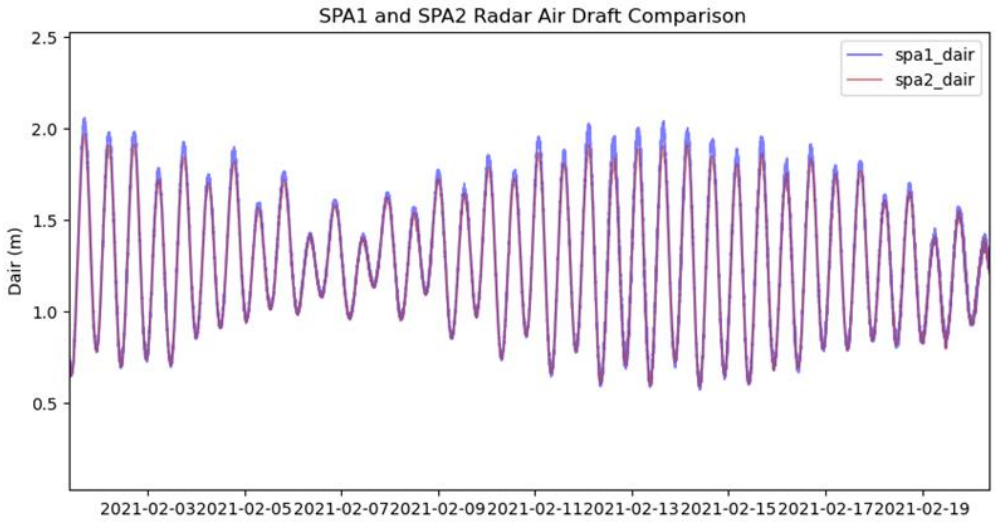

Figure 13 : SPA1_RDR truncated signal example occurring during 2020

- SPA2 radar gauge (SPA2_RDR) data quality check

The SPA2 radar measurements are continuous over all the period of analysis between December 2018 and March 2023. We have noticed an increase of the outlier occurrence at high tide since September 2022 in the transmitted data. The comparison with the SPA2 memory do not show any outliers as illustrated in Figure 14, which indicates an issue with the Argos transmission that must be solved during a next NIVMER operational mission on site.
The cleaning of the SPA2 tide gauge raw data consists of removing outliers standing above three times the standard deviation of the overall tide gauge measurements.

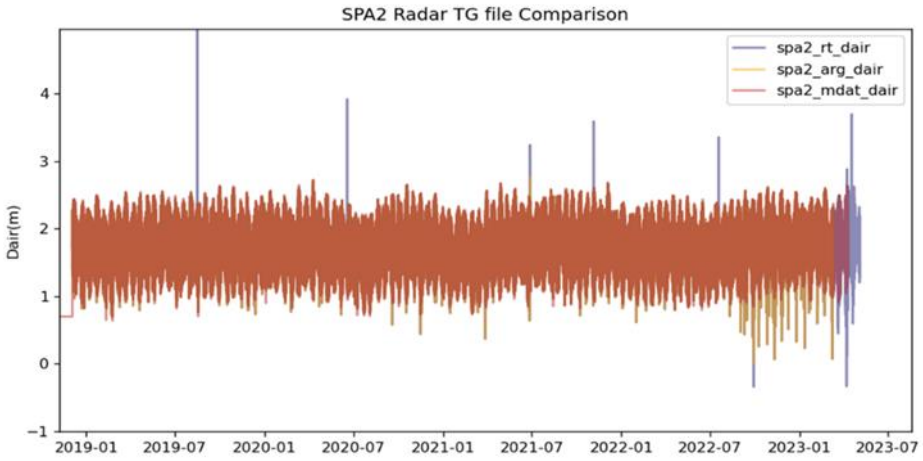

Figure 14 : Example of SPA2 suspicious peaks occurring since mid-2022 for "argos" file data in orange and real-time data in blue; station memory data collected mid-April 2023 are in brown.

3.5.2 Bottom Pressure tide gauge data

The sea level measurements η_{BPR} from the bottom pressure gauges are calculated from the difference between the bottom (Pb) and the atmospheric (Pa) pressure following the formula:

$$\eta_{BPR} = \frac{P_b - P_a}{\rho . g}$$

η_{BPR}: the instantaneous bottom pressure sea level (m)
P_b : bottom pressure (Pa)
P_a: atmospheric pressure (Pa)
ρ : ocean water density (kg.m−3) computed with constant salinity (34 psu)
g : local gravity acceleration (m.s−2) defined as function of the latitude and equals to 9.78 in Saint-Paul.

The BPR sea level referenced to Zh_LEGOS is given by adding the levelling estimate of measurement reference point (Zm) of the bottom pressure gauge (SPA1_BPR):

$$\eta_{Zh\_BPR} = \eta_{Zh\_BPR} + Zm$$

where *Zm* is 0.607 m.

The pressure gauge, widely used for sea level measurement since the 60's, have some disadvantages such as difficulties in controlling their datum and the sensor drift as reported in several studies (Miguez et al. (2012); Testut et al. (2006); Woodworth et al. (1996)). The well-known bottom pressure sensor drift requests therefore a calibration every six months, which cannot be performed in remote sites such

Saint-Paul Island for which maintenance visits occur mainly once a year and for few hours. The sensor drift will be estimated from the sensor inter-comparison analysis.

The other issue is the bottom pressure datum used for the analysis period 2018-2023 in the present study. The last available levelling information for the bottom pressure tide gauge is from 2010 followed by several bottom pressure tide gauge maintenance such as the sensor cleaning or change. Therefore, a large uncertainty exits regarding the sensor datum, which has to be as well investigated through the sensor inter-comparison analysis.

The raw data are cleaned from the outliers defined as all the data above three times the standard deviation.

3.5.3 GNSS reflectometry (GNSS-IR)

In Saint-Paul Island, the GNSS Interferometry approach, as a secondary use of the GNSS receiver (SPTG) installed on the stilling tube structure, allows to retrieve the sea level height from the GNSS reflections off the sea surface. The GNSS Interferometry data processing is performed by PSMSL and the GNSS reflectometry data are available from the portal (https://psmsl.org/data/gnssir/site.php?id=10261).
Since early 2022, the Saint-Paul GNSS receiver can typically record data from all current GNSS systems (e.g., GPS, Glonass, Galileo) and multiple frequencies, which significantly increase the amount of sea level retrievals available per day.

The GNSSIR air draft is obtained according to:

$$Dair_{GNSSIR} = RH + Hdot$$

RH: Reflector Height, which is an estimate of the average height of the receiver's phase centre above the water below.
Hdot: mean rate of change of the tide during the satellite arc predicted from the tidal fit.

The GNSSIR sea level is given by subtracting the air draft to the levelling estimate of the GNSS-ARP (Antenna Reference Position) referenced to Zh_LEGOS:

$$\eta_{Zh\_GNSS} = GNSS_{Zh} - Dair_{GNSSIR}$$

where $GNSS_{Zh}$ is 3.493± 0.001 m.

However, it is important to notice that the reference point of the GNSS measurement is the Antenna Face Center (AFC) (Figure 15), which will be estimated from the sensor inter-comparison analysis.

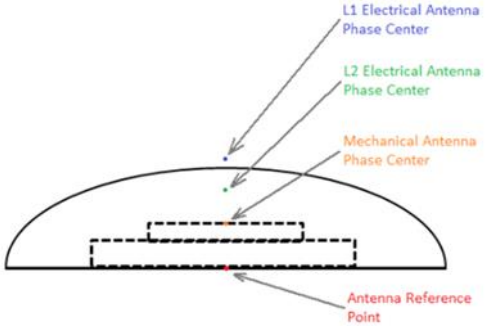

Figure 15 : GNSS antenna diagram with the different Antenna Phase Centers (AFC) and Antenna Reference Point (ARP) (ref: https://receiverhelp.trimble.com/alloy-gnss/en-us/AntennaPhaseCenters.html)

In addition, the GNSS antenna has been installed at the tide gauge for ease of access; however, this position is located in mask environment and it had a limited view of the water, which is far from optimal as illustrated with the Fresnel zone in Figure 16-A. The inter-comparison analysis will be performed for the whole Fresnel, and with a filter on the azimuth between 0-150° and 150°-260° to investigate a potential impact of the accuracy of the result. Figure 16-B displays the Fresnel zone with an azimuth filter between 150° and 260°.

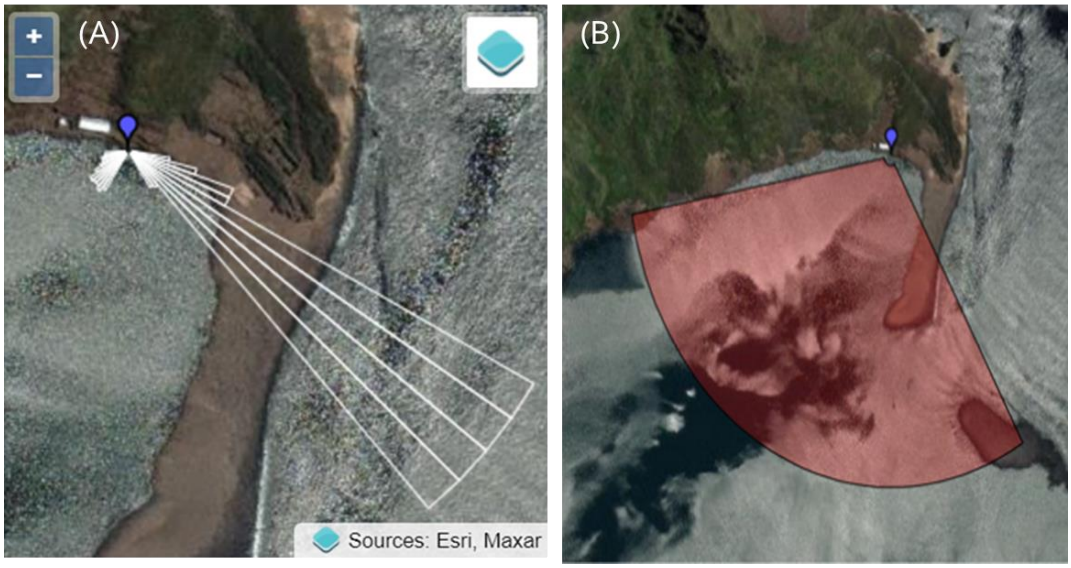

Figure 16: (A) Satellite view of Saint-Paul site with GNSSIR Fresnel zones according to the elevation angle and antenna height;; (B) Filter zone applied according to the azimuth: 150°< Azi <260° (https://psmsl.org/data/gnssir)

3.6 Vertical Land Movement Measurement

In Saint-Paul Island, the precise levelling and space geodesy are the two sources of data that can provide information on land motion. An analysis of the levelling differences between the 1994, 2010 and 2018 campaigns shows that a height difference of 10 ± 1 mm is reported between the intermediate benchmarks C and the geodetic reference benchmark D, which could be due either to a vertical land movement or a levelling error in 2010 campaign.

In addition to the precise levelling, space geodesy data available since 2012 can provide additional information on land motion affecting Saint-Paul site in a global reference frame. The GNSS processed data by La Rochelle University and Nevada Geodesy Laboratory are accessible from SONEL website (www.sonel.org). Figure 17 displays the GNSS vertical component displacement provided by Nevada Geodesy Laboratory version, which has the longer time coverage.

SONEL website mentions potential offsets in the GNSS vertical displacement linked either to earthquake (red) or to maintenance on the GNSS antenna. The last GNSS antenna maintenance in Dec 2018 not mentioned in SONEL site has been added in this plot and corresponds to the new antenna position in December 2018. The new position was move up by 41 ± 1 mm relative to 2014 position; this shift does not seem to fit with the observed offset between 2014 and 2018. Further investigations have to be

performed to quantify the Saint-Paul vertical land movement due to seismic activity, which is out of the scope of the present study.

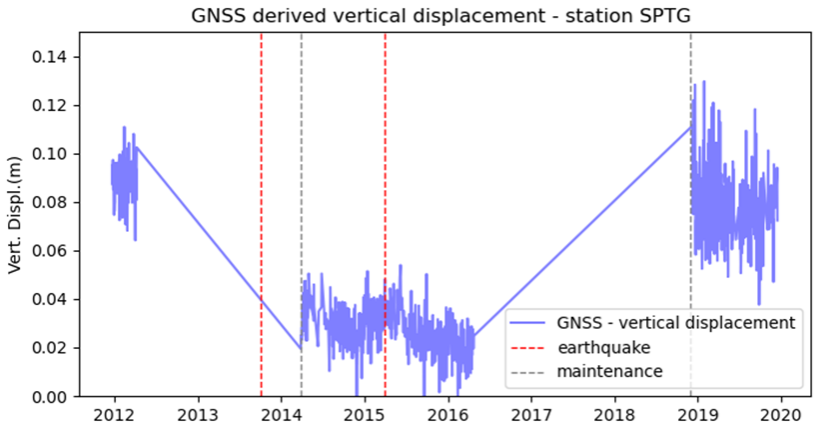

Figure 17 : Saint-Paul GNSS vertical component displacement

4 Sensor data inter-comparison

The inter-comparison between the different records will allow us to detect systematic deviations such as bias, drift and assess the sensor data quality through tidal constituents, time serie differences and Van de Casteele method. In this section, we will investigate as well the ability of GNSS reflectometry technique (GNSSIR) to measure sea level variation for Saint-Paul Island.

4.1 Tidal Constituents from Harmonic Analysis

To separate the tidal from the non-tidal component of the observed total water elevations, the harmonic tidal analysis method is used. In this approach the tidal component is represented as a set of sinusoids at specific tidal frequencies (Pugh, 1987). The longer the record, the more sinusoids with closely related frequencies can be discriminated. A least-squares fit is then used to determine the coherent relative phase and amplitude of each tidal frequency within the total elevation, the remaining signal (the residual) is assumed to be non-tidal.

A harmonic analysis of the time series provided by each sensor was performed using Python Utide program. The results for the five main tidal constituents are presented in Table 2, Table 3 and Table 4 for the years: 2020, 2021 and 2022, respectively. For the year 2020, the amplitudes of the 5 main semi-diurnal tidal constituents for SPA2_RDR and SPA1_BPR presents similar amplitudes and phases whereas the amplitude of M2 and S2 for SPA1_RDR and SPA-GNSSIR are significantly lower than for SPA2_RDR and SPA1_BPR. Differences in phase between sensors occur for the tidal constituent N2 and K1.
Comparing tidal constituent properties between years indicates a stability in their estimate for SPA2_RDR, SPA1_BPR and GNSSIR sensors, whereas GNSSIR has its tidal constituents' amplitudes always lower than SPA2_RDR and SPA1_BPR. Regarding SPA1_RDR sensor; the significant difference in the M2 and S2 tidal amplitudes estimates between both periods arise question regarding the reliability of the sensor in the tidal magnitude prediction. Only in 2022, the tidal constituents of SPA1_RDR are in a comparable order with SPA1_RDR. This issue could be related to a scale error factor affecting SPA1_RDR sensor and will be investigated through the other inter-comparison methods.

Table 2: The 5 main tidal constituents at Saint-Paul Island for the period Jan. 2020 – Dec. 2020

Main Tidal Constituents	SPA1_RDR		SPA2_RDR		SPA1_BPR		SPA_GNSSIR	
	Ampl. (m)	Phase (deg)	Ampl. (m)	Phase (deg)	Ampl. (m)	Phase (deg)	Ampl. (m)	Phase (deg)
M2	0.381	230	0.398	230	0.399	230	0.376	230
S2	0.202	272	0.215	274	0.212	273	0.203	275
N2	0.067	152	0.072	211	0.074	212	0.085	140
K1	0.066	205	0.071	153	0.070	152	0.066	213
K2	0.053	281	0.060	273	0.060	273	0.032	255

Table 3: The 5 main tidal constituents at Saint-Paul Island for the period Jan. 2021 – Dec. 2021

Main Tidal Constituents	SPA1_RDR		SPA2_RDR		SPA1_BPR		**SPA_GNSSIR**	
	Ampl. (m)	Phase (deg)	Ampl. (m)	Phase (deg)	Ampl. (m)	Phase (deg)	Ampl. (m)	Phase (deg)
M2	0.417	230	0.398	230.4	0.398	230	0.378	230
S2	0.223	274	0.215	274.0	0.213	273	0.201	273
N2	0.075	211	0.075	212.1	0.073	212	0.078	211
K1	0.069	151	0.069	152	0.070	151	0.069	150
K2	0.062	269	0.061	272	0.060	272	0.033	280

Table 4: The 5 main tidal constituents at Saint-Paul Island for the period Jan. 2022 – Dec. 2022

	SPA1_RDR		SPA2_RDR		SPA1_BPR		**SPA_GNSSIR**	
	Ampl. (m)	Phase (deg)	Ampl. (m)	Phase (deg)	Ampl. (m)	Phase (deg)	Ampl. (m)	Phase (deg)
M2	0.402	230.3	0.397	230.1	-	-	0.379	230
S2	0.219	274.0	0.215	273.8	-	-	0.205	272
N2	0.076	213.4	0.074	213.1	-	-	0.074	213
K1	0.071	152.3	0.070	151.7	-	-	0.070	145
K2	0.062	272.2	0.061	272.1	-	-	0.047	275

4.2 Time Serie Difference

Another sensor inter-comparison tool is the visualisation of the sea level difference by couple of sensors. The instantaneous sea level data of each sensor are referenced to ZH_LEGOS based on the levelling information and are subtracted to each other based on a signal processing decimation.

- SPA1_RDR and SPA2_RDR

Figure 18 displays the instantaneous sea level differences between SPA1_RDR and SPA2_RDR relative to Zh_LEGOS, on which events regarding the stilling tube and SPA1 sensor cleaning maintenance are

marked. Based on the observation of the sea level difference time series, four sub-windows were determined based on site maintenance dates or data recording interruption: Dec. 2018, Dec. 2019-Nov.2020, Nov.2020-Dec.2021 and Dec.2021 – Mar.2023. A computation of simple statistical descriptors: mean, median, standard deviation, maximum, minimum by the sub -windows are summarized on Figure 18 (Left).

Over the period Dec.2019 – Nov.2020, as mentioned in section 3.5.1, the SPA1 radar is impacted by the stilling tube obstruction, which increases significantly the standard deviation to 45 mm. The sea level difference median value of 1 mm indicates that the sensors positions agree with the levelling information provided in Dec. 2018 and applied to the overall period 2018-2023 to obtain the Zh_LEGOS referenced sea level and fit with the levelling uncertainties of 1 mm. The levelled radar sensor offset is 0.371 m based on the December 2018 levelling campaign and confirmed in April 2023 mission. No levelling operation was done from 2018 onwards.

From November 2020 with the rod detangling maintenance, we observe a reduction of the dispersion of the sea level differences, with a standard deviation decreasing to 18 mm after the SPA1 radar sensor cleaning in December 2021. On the other side, in Figure 18 (Right), the monthly boxplot of sea level difference highlights that over the period Dec. 2020- Dec.2021, a shift upward of the sea level difference mean to 17 mm, which get reduced and improved after the SPA1 radar cleaning in December 2021 and in April 2022. Since no maintenance were performed on the open-air SPA2 radar, we can deduce that the maintenance operations on the sensors inside the stilling tube even done carefully have an impact on the standard deviation of the sea level differences (from 43 mm to 19 mm) and on the offset between the two sensors. Therefore, the SPA1 vertical position need to be corrected by the median value (17mm) over the period Dec.2020-Dec. 2021 in absence of levelling information to be able to compute a mean sea level from this sensor.

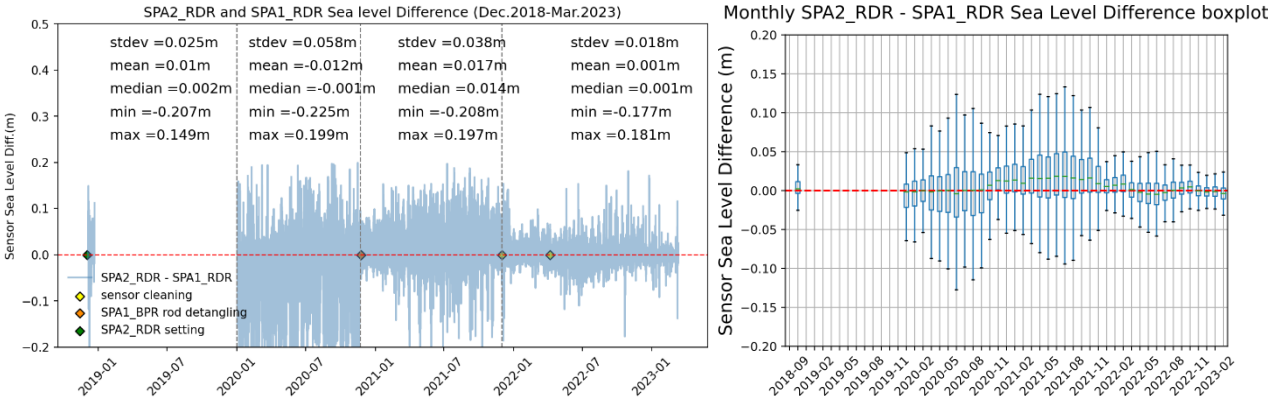

Figure 18 : (Left) Sea level difference between SPA2_RDR and SPA1_RDR with the sensor and stilling tube maintenance marks; (Right) Monthly boxplot of the sea level difference between SPA2_RDR and SPA1_RDR

- SPA1_RDR and SPA1_BPR

Figure 19 displays the instantaneous sea level differences between SPA1_RDR and SPA1_BPR relative to Zh_LEGOS. The sea level difference indicates a limited standard deviation of the measurement, which varies between 10 mm and 24 mm over the period Dec. 2018 and Jan. 2022, which nevertheless tends to increase over the year 2022. Considering the sea level difference median, the values above 160 mm before Nov. 2020 and 129 mm afterwards indicate a serious disagreement with the levelling information. Since the SPA1 radar and SPA2 radar comparison agrees with the levelling information outside of the period Nov. 2020- Dec.2021, this implies that the SPA1 bottom pressure sensor information is not set-up at its last levelling position established in 2010. This is entirely possible knowing that the tide gauge has been removed from the stilling tube several times since 2010 as mentioned in Figure 4. In addition, the rod detangling maintenance in Nov. 2020 affects the sea level difference by a generating shift down of the time series well illustrated in the monthly boxplot in Figure 19 (Right). This shift is estimated at 47 mm from the 3 monthly median averages before and after the maintenance

event. Beside the time series shift down, the monthly box plot in Figure 19 highlights an increase of the monthly mean of the sea level difference between Nov.2020 and Jan.2022, which could be associated to a drift of the bottom pressure tide gauge. This drift was calculated from the trend estimation from the least square method and equals 24 mm/y ± 1 mm/y at 95% confidence interval ($p < 0.05$).

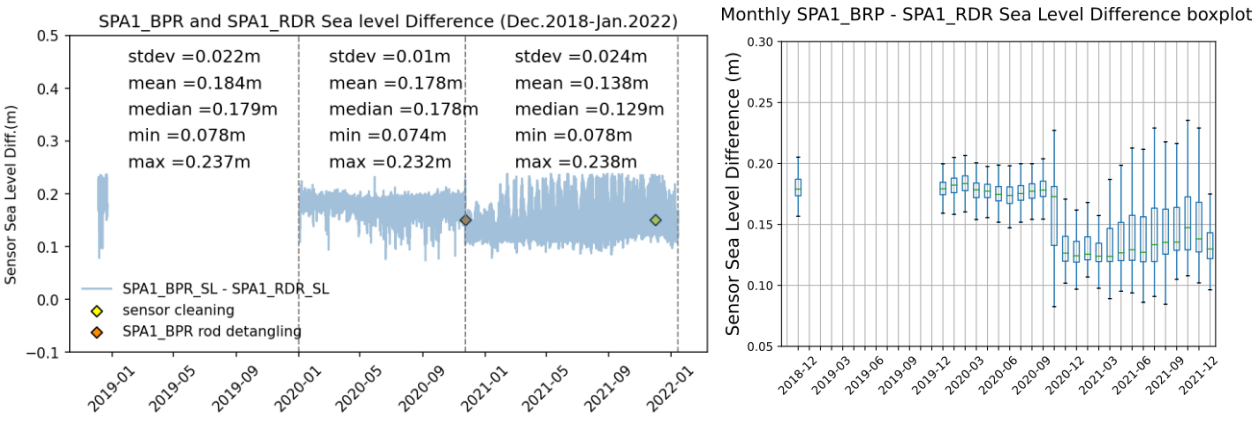

Figure 19 : (Left) Sea level difference between SPA1_BPR and SPA1_RDR with the sensor and stilling tube maintenance marks; (Right) Monthly boxplot of sea level difference between SPA1_BPR and SPA1_RDR

- SPA1_RDR and GNSS-IR

The comparison with SPA1_RDR was performed for the full GNSSIR dataset and for filtered GNSSIR datasets based on azimuth threshold of 150°deg. The sea level difference is done on daily mean and is displayed in Figure 20 for the full GNSSIR dataset and the GNSSIR dataset with an azimuth greater than 150°deg. The GNSSIR measurements show a good agreement with the SPA1_RDR gauge, exhibiting a standard deviation of 34 mm for full GNSSIR dataset and of 33 mm for the filtered GNSSIR dataset. By considering the GNSSIR data with an azimuth greater 150° and computing the monthly mean, the standard deviation decreases to 11 mm, which is a very good result. In addition, the median value provides us the information about the height of the Antenna Phase Centre, which has to be used as measurement reference. This bias correction has to be applied to GNSSIR dataset.

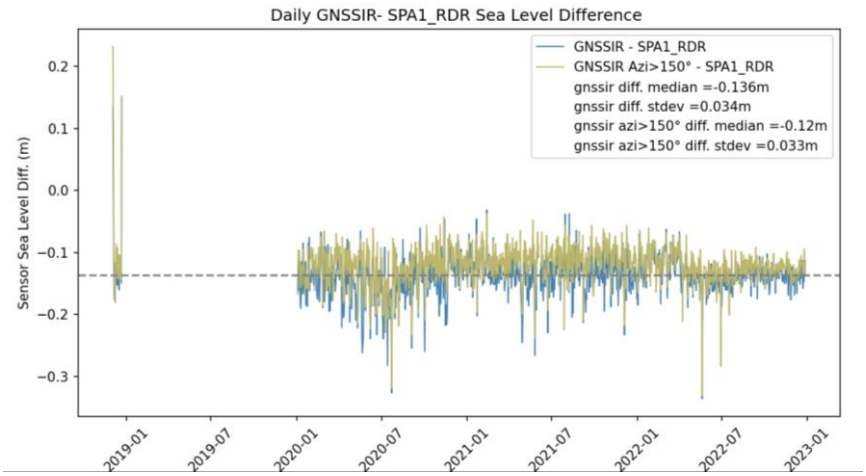

Figure 20 : Sea level difference between SPA1_RDR and GNSSIR for the full dataset and by applying a filter on the azimuth

- SPA2_RDR and SPA1_BPR

Similar aspects occurring for the sensor couple: SPA1-RDR / SPA-BPR happen to the sea level difference between SPA2_RDR and SPA1_BPR sensors. Thus, a shift down of the timeseries is observed as well in Nov. 2020 and is estimated to 49 mm using the similar calculation previously (Figure 21). The drift of the monthly mean after Nov. 2020 equals to 24 mm/y ± 1 mm/y at 95% confidence interval ($p < 0.05$). The shift and bottom pressure drift estimated for the sensor couple SPA2_RDR / SPA1_BPR agree with the ones computed for the sensor couple: SPA1-RDR / SPA-BPR. In addition, from the monthly boxplot, we can observe that the standard deviation tends to increase with time from December 2018 to November 2020 while the median is relatively constant. A possible explanation could be the lack of maintenance of the bottom pressure gauge or the stilling tube since the rod detangling maintenance improve significantly the standard deviation post November 2020.

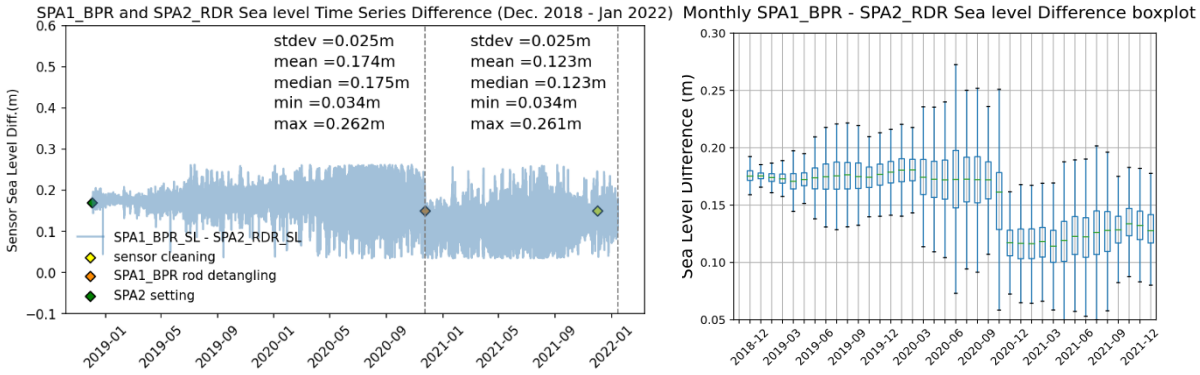

Figure 21 : (Left) Sea level difference between SPA1_BPR and SPA2_RDR with the sensor and stilling tube maintenance marks; (Right) Monthly boxplot of the sea level difference between SPA1_BPR and SPA2_RDR

- SPA2_RDR and GNSS-IR

The comparison with SPA2_RDR was done for the full GNSSIR dataset and for the filtered GNSSIR datasets based on azimuth threshold of 150°deg. The daily sea level difference is displayed in Figure 22 for the full GNSSIR dataset and the GNSSIR dataset with an azimuth greater than 150°deg. The GNSSIR measurements show a very good agreement with the SPA2_RDR gauge with a standard deviation of 32 mm for full GNSSIR dataset and of 27 mm for the filtered GNSSIR dataset in spite of the Saint-Paul environment. By filtering the GNSSIR according to the azimuth (azi > 150°) and considering the monthly mean, the computed standard deviation exhibits a value of 7mm. Therefore, the use of the GNSSIR to analyse the sea level variation on monthly basis is as monitoring.

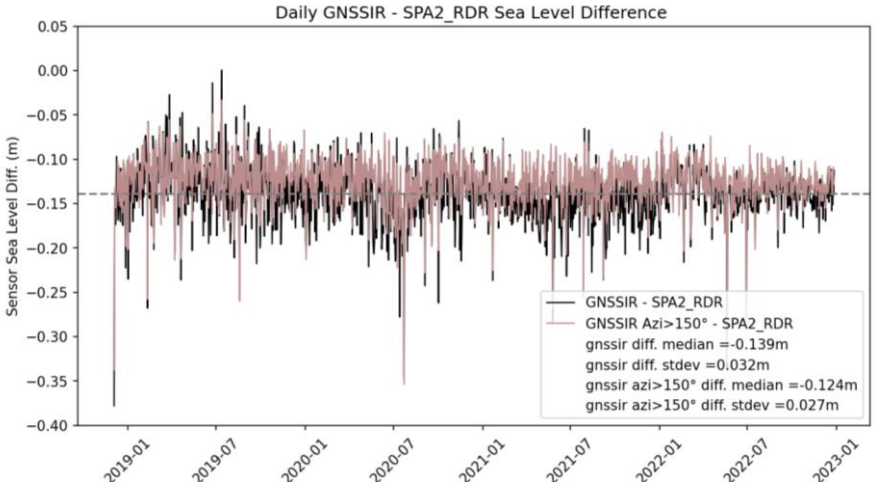

Figure 22 : Daily sea level difference between GNSSIR and SPA2_RDR

4.3 Van De Casteele Plot

In order to assess the quality of the different tide gauges, the Van de Casteele test (VDC) is used in this study. This test enables us to characterize the errors of the tide gauges. The purpose of the VDC test is to compare the measurement of the sensor under test with a reference gauge, like tide pole readings; the two devices have to be located in a same place or close enough so that the signals are very similar. Since both sensors should measure the same sea level, the difference between the two sensors should be zero or at least constant over time, regardless of the amplitude of the measurement. In this comparison method, the Van de Casteele diagram plots the difference between the two sea level measurements referenced to a same geodetic benchmark: DH = H' – H as function of H, in which H' is the measurement of the sensor under test and H is the reference sensor one. Appendix B displays type of tide gauge error identification and the associated VDC plots (Lenon (1968); Miguez et al. (2005))
In our study, no reference gauge in saint-Paul Island is established yet and the VDC plot has to enable us to define it. However, based on past tide gauge inter-comparison analysis (Woodworth (2003); Miguez et al. (2005, 2012); Testut et al. (2006)), the radar tide gauge technology has shown good results in terms of precision and stability of the measurement. Therefore, for the VDC plots analysis, two sets of comparison are carried out with SPA1_RDR and SPA2_RDR as reference sensor. A fitting is performed between DH as function of H using either a second degree polynomial or a firstdegree polynomial fitted with the least square in order to estimate any scale error. The distinction between flood and ebb data is performed as well. A bias is computed as the mean of the difference of the sea level between sensors DH over the considered time window.

- VDC plots with SPA1 _RDR as reference

Figure 23 (a, b, c) displays the VDC plots using SPA1_RDR as reference and SPA2_RDR, SPA1_BPR and GNSSIR as test sensors on a week window, respectively. Over the different plots, we can notice the dispersion of the data cluster is variable with more noise occurring for the sensors outside the stilling tube: SPA2_RDR and GNSSIR than for the sensor SPA1_BPR setting up in the well. In addition, for the SPA2_RDR test sensor, we can notice a shift in the data cluster between the ebb and the flood time indicating a sea level magnitude issue for either the reference sensor or the test sensor (Figure 23 (a) and (b). Considering the polynomial fitting of DH as function of H, we do not obtain a straight vertical fitting line aligned with the zero-bias reference line, which indicates an instrumental issue. For the test sensors SPA2_RDR and SPA1_BPR (Figure 23 (a) and (b), we can notice that a vertical fitting line is occurring at high tide for sea level above 2 m. At low tide, we are getting an inclination of the fitting line, which impact the bias computation. For the GNSSIR sensor (Figure 23 (c)), independently from the tide, the linear least squares fitting line is inclined. Therefore, a scale error is suspected to belong to SPA1_RDR sensor since it is a common denominator to all the VDC plots. Finally, the last observation, which can be made, concerns the estimated bias. For SPA2_RDR / SPA1_RDR couple, the bias equals – 4 mm at high tide, which indicates a relatively good agreement with the levelling sensor position. The bias of 17 mm for GNSSIR SPA1_RDR couple is partially due to the reference point of the GNSSIR measurement, which have to be established. On the other side, for SPA1_BPR / SPA1_RDR couple, the bias is estimated at 117 mm at high tide, which emphasises an offset between sensor. This offset disagrees with the levelling information used to reference the SPA1_BPR sensor.

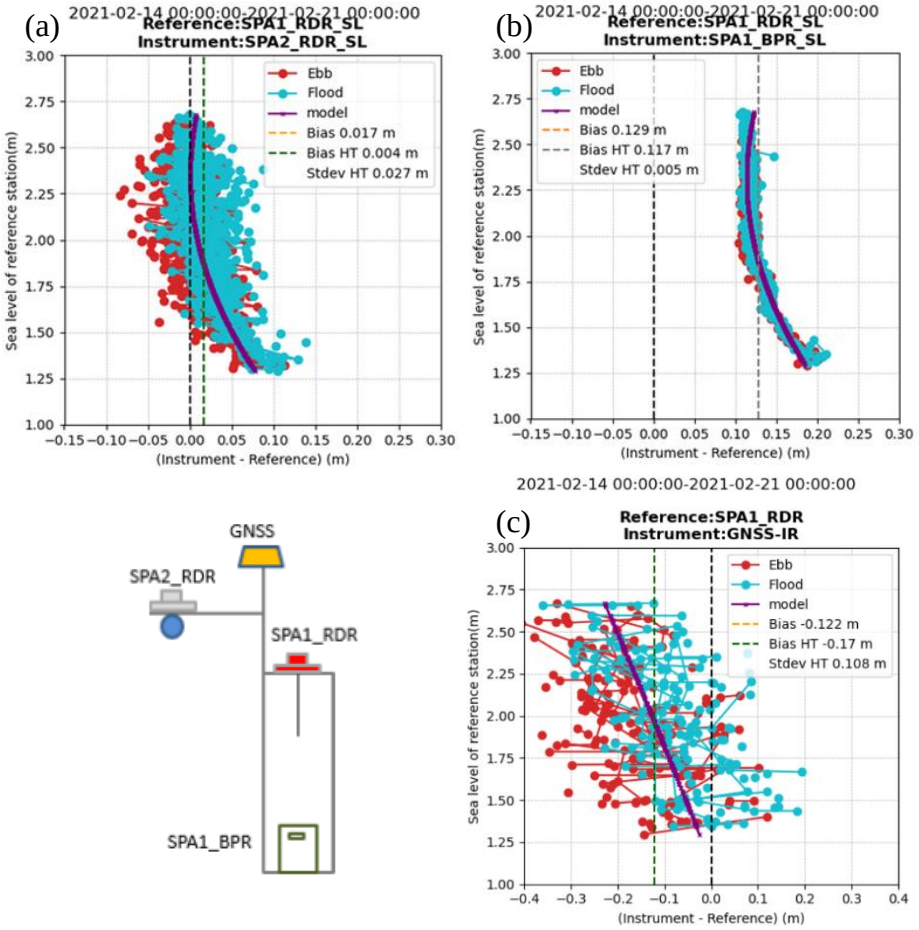

Figure 23 : Weekly based VDC plots with SPA1_RDR as reference gauge and SPA2_RDR (a), SPA1_BPR(b) and GNSSIR (c) as test sensors

- VDC plots with SPA2 _RDR as reference

Figure 24 (a, b, c) displays the VDC plots using SPA2_RDR as reference sensor and SPA1_RDR, SPA1_BPR and GNSSIR as test sensors on a week window, respectively. The major additional information is obtained from the VDC plot for the SPA2_RDR / SPA1_BPR couple (Figure 24 b), for which the least squares fitting is completely straight and vertical. This implies that the instrumental issue encountered at low tide comes from the SPA1_RDR sensor. In addition, a slight shift of the data occurs between the ebb and the flood event for the SPA2_RDR / SPA1_BPR couple (Figure 24 b), which was not the case for the SPA1_RDR / SPA1_BPR couple. This difference between VDC plots indicates that the set-up condition between SPA2_RDR in open-air and the other sensors SPA1_BPR and SPA1_RDR being at the stilling tube, affects the sea level measurement between ebb and flood. Regarding the GNSSIR test sensor, the inclined linear least square fitting curve indicates that the GNSSIR suffers from a scale factor error, which have to be corrected.

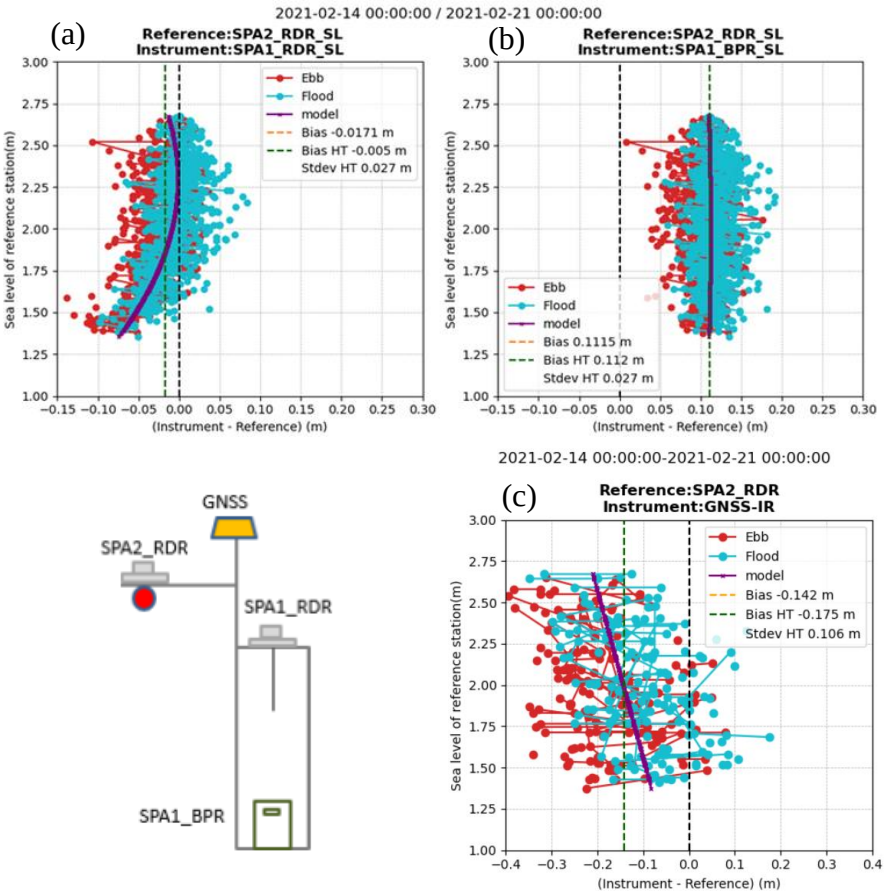

Figure 24 : Weekly based VDC plots with SPA2_RDR as reference gauge and (a) SPA1_RDR, (b) SPA1_BPR and (c) GNSSIR as test sensors

- Bias evolution from VDC plots

Figure 25 and Figure 26 illustrate the VDC derived bias evolution relative to SPA1_RDR and SPA2_RDR, respectively, used as reference sensor for the different sensor couple combinations over 2021. We are differentiating the bias for the full signal from the high tide signal based on the VDC observations, especially for sensor couple involving SPA1_RDR. We can observe that the slopes for the different couples of sensors are different between the full signal and the high tide signal, except for the SPA2_RDR/SP1_BPR couple. The bias for the SPA1_RDR/SPA2_RDR couple is constant over time and almost null. However, the associated standard errors to the predicted slopes for the sensor couples: SPA1_RDR/SPA2_RDR and SPA1_RDR/GNSSIR are large regarding the estimated slope value; the statistics for both couples are non-significative (probability $p > 0.05$). For SPA1_RDR/SPA1_BPR couple, an increase of the bias over 2021 is observed with a slope of 26.8 ± 2.2 mm/y for the entire signal and 13.2 ± 2.0 mm/y for the high tide signal at 95% of confidence interval ($p < 0.05$). The calculated slope for the full signal is aligned with the drift calculated in the time series difference: 24 mm/y ± 1 mm/y.).

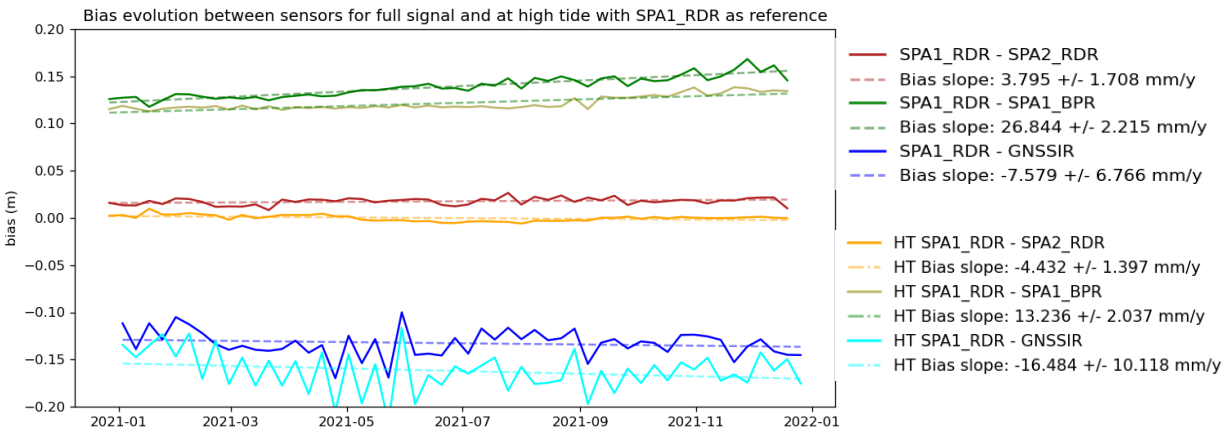

Figure 25 : VDC derived bias evolution relative to SPA1_RDR for the entire sea level signal and at high tide for the different sensor couples: SPA1_RDR / SPA2_RDR, SPA1_RDR/ SPA1_BPR and SPA1_RDR / GNSSIR

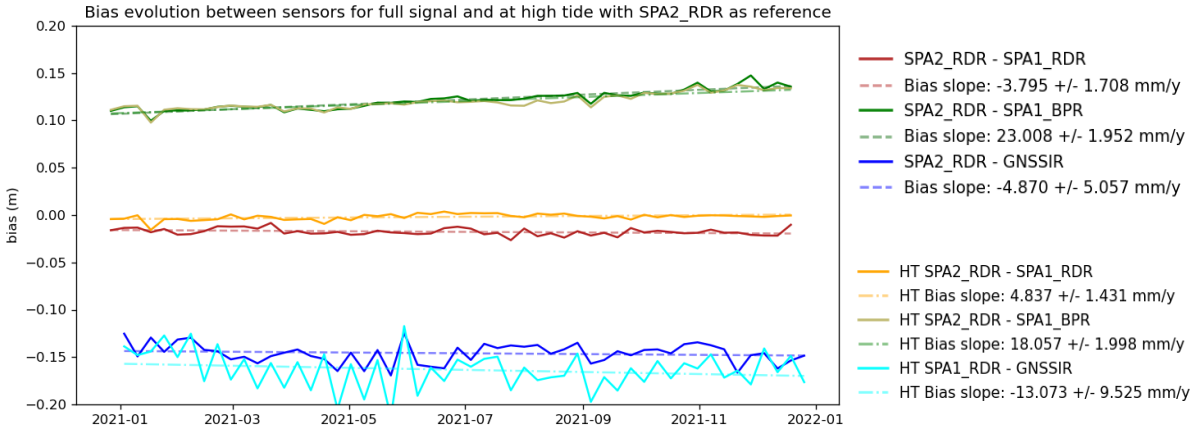

Figure 26 : VDC derived bias evolution relative to SPA2_RDR sensor for the entire sea level signal and at high tide for the different sensor couples: SPA2_RDR / SPA1_RDR, SPA2_RDR/ SPA1_BPR and SPA2_RDR / GNSSIR

- Scale factor

The scale error for SPA1_RDR occurs between December 2020 and December 2021, which is linked to site maintenance. The scale error correction to apply is defined from a second degree polynomial fitted by least square method. Figure 27 shows the evolution of the coefficients of the polynomial fitting:

$$H - H' = C + B * H' + A * H'^2$$

in which H is the SPA2_RDR reference instrument and H' is the SPA1_RDR instrument to correct. The polynomial coefficients are relatively constant over time. The SPA1 sea level data corrected from the scale error are obtained by applying the following correction:

$$H'corr = H' - (C + B * H' + A * H'^2)$$

Figure 27 (Right) displays the VDC after correcting the scale error of SPA1_RDR measurement over 2021. A similar process has been applied to the GNSSIR data by using a first order polynomial fitting.

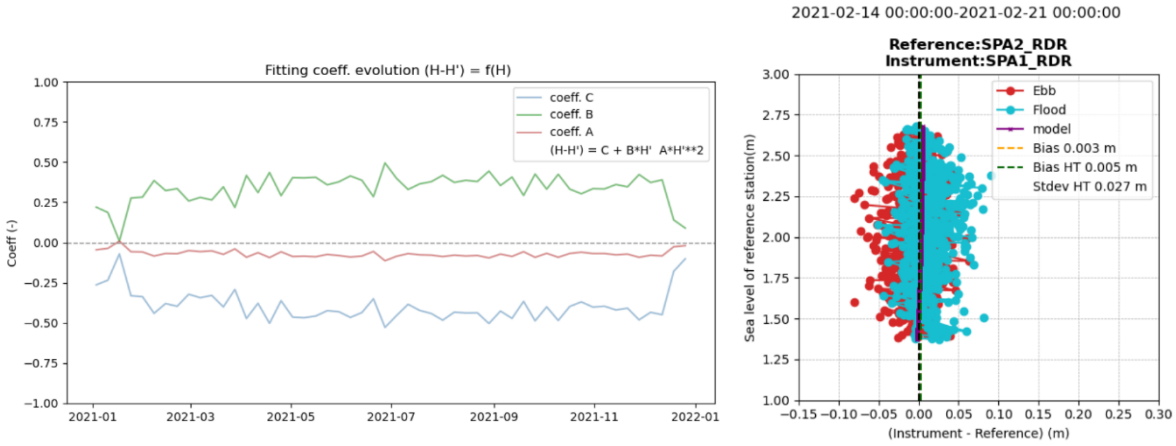

Figure 27 : (Left) evolution of the second-degree polynomial coefficients over 2021 fitted with least square method; (Right) VDC with the SPA1_RDR sensor after correcting the scale error

5 Discussions and Conclusion

Calibrations and comparisons of the sea level data sets are essential to assess the quality of the data and to ensure their usefulness for applications like the mean sea level trend. Testut et al. (2010) analysis uses the spatial altimetry and GNSS buoy to calibrate the tide gauges (SPA1_BPR and SPA1_RDR) and determine a mean sea level trend from 1874. Since then, the remote Saint-Paul station get enriched with an open-air tide gauge (SPA2 radar tide gauge) and GNSS permanent station. In this context, longer period of sensor working simultaneously and time synchronised enable us to carry multi-sensor inter-comparison for the period 2018-2023 in order to appraise the data quality, to establish a reference gauge and to investigate the potential of the GNSS interferometry for the sea level measurement in Saint-Paul site.

The multi-comparison has emphasised different sources of uncertainties in the sea levels measurements, which have been quantified. One common source of error is related to the tide gauges measuring different tidal ranges (also scale error factor). This scale error has been detected for the SPA1 wave guided radar gauge (SPA1_RDR) between 24 Nov.2020 to December 2021 for low tides; both dates correspond to maintenance operation on stilling tube and SPA1 radar gauge: SPA1_BPR rod detangling and SPA1_RDR cleaning from algae's, respectively. This informs us on the critical impact of the maintenance over the sea level measurements in positive or negative ways. From the sea level time series difference, the standard deviation between sensors involving SPA1_radar get reduced significantly and no more scale factor was present after the SPA1 wave guided radar cleaning in December 2021. For the GNSSIR data, the source of the scale factor error, which is rather permanent over the period of the study, might be related to the context of installation of the GNSS antenna in an environment with mask, which can affect the number of reflected height data retrieved from the satellite constellation and their quality.

Another source of important uncertainty inherent to the limited access and short maintenance duration in Saint-Paul is the sensor bias due to a lack of levelling of the contact point of the different sensors after maintenance operations. This aspect concerns the SPA1 bottom pressure gauge and the SPA1 radar tide gauge, which have been removed several times either to be replaced or cleaned after levelling campaigns. Sensor inter-comparison enables us to correct the bias associated with changes in the gauge contact point using the SPA2 radar gauge as reference. Regarding the GNSSIR, its bias is directly linked to its Antenna Phase Center estimate; its exact position is initially unknown and established after carrying out the inter-comparison analysis.

The sensor drift can represent an important error is sea level measurement and concerns atmospheric and bottom pressure sensors. In case of Saint-Paul site, in spite of a significant barometric drift identified over the period 1994 – 2007, the installation of the new a barometric sensor associated to DT-INSU station has erased this drift, which has been confirmed by the estimation of the non-significant drift between Saint-Paul data and Amsterdam meteorological data. On the other side, bottom pressure tide gauge can drift an order of magnitude of 24 ± 1 mm/y between November 2020 and January 2022, which is greater than sea level trend of -0.1 ± 0.3 mm/y estimated by Testut et al (2010). The monitoring of bottom pressure sensor drifts in site with limited access for maintenance as Saint-Paul questions the reliability of data for sea level trend estimate in absence of other sensors on site.

Based on the inter-comparison analysis, our results showed the reliability of the open-air SPA2 radar sensor in terms precision and stability, particularly when compared with the SPA1 radar gauge and SPA1 bottom gauge either prone to scale factor error or bias or drift. The open air SPA2 does not request regular cleaning typical to the gauges installed in the stilling tube and thus is less subject to have a change in its contact point. On the other side, the SPA2 radar gauge does not beneficiate from the filter role of the stilling tube. Ebb and flood events could be distinguished in SPA2 radar gauge measurement.

The ability of GNSS reflectometry approach (GNSSIR) to measure sea level variation for Saint-Paul Island was investigated in this study. The comparison with the SPA2 reference radar tide gauge shows that the GNSSIR sea level measurements are in good agreement with a standard deviation of 2.7 cm for the daily mean; this standard deviation gets optimised with the monthly mean and filtering the GNSSIR with an azimuth greater than 150° deg. Knowing that the Saint-Paul environment presents mask and is not optimal for reflectometry approach, we could expect that a GNSS antenna set-up in open environment will provide even more promising results for the sea level monitoring.

In conclusion, the present study contributes to a better understanding of the performance of Saint-Paul tide gauges and their stability. Based on the inter-comparison analysis, we were able to identify sensor errors and quantify their magnitudes. These errors can be either inherent to the sensor like the bottom pressure gauge drift or due to the restrictive access to Saint-Paul natural limiting a good site maintenance. Our results showed the superiority of the SPA2 open-air radar sensor in terms of stability, especially for remote site with limited maintenance like Saint-Paul. Furthermore, GNSSIR approach is a promising and could be an alternative way to tide gauge for measuring the sea level measurement. However, it will most likely require to set-up a GNSS antenna in an open environment to assess all its potentiality in sea level monitoring. The study also evidenced that no technology is free from and having several tide gauges operating simultaneously and different storing -transmission support is worthwhile, especially for remote site like Saint-Paul Island.

6 References

Church, J.A. and White, N.J. (2006) 'A 20th century acceleration in global sea-level rise: AN ACCELERATION IN GLOBAL SEA-LEVEL RISE', *Geophysical Research Letters*, 33(1), p. n/a-n/a. Available at: https://doi.org/10.1029/2005GL024826.

Holgate S;J., Matthews A. , Woodworth P.L., Rickards L.J., Tamisiea M.E., Bradshaw E. , Foden P.R., Gordon K.M. , Jevrejeva S., and Pugh J. (2013), New Data Systems and Products at the Permanent Service for Mean Sea Level, *Journal of Coastal Research*, vol 29-3, 493–504

Intergovernmental Oceanographic Commission (IOC) (2006), Manual on sea level measurements and interpretation, vol. 4: An update to 2006, in IOC Manuals and Guides No. 14, 80 pp., *U. N. Educ. Sci. and Cult. Org.*, Paris.

Larson, K.M., J. S. Lofgren, and R. Haas (2013) 'Coastal sea level measurements using a single geodetic GPS receiver', *Adv. Space Res.*, 51, 1301–1310. Available at: https://doi.org/10.1016/j.asr.2012.04.017

Larson, K.M., Ray, R.D. and Williams, S.D.P. (2017) 'A 10-Year Comparison of Water Levels Measured with a Geodetic GPS Receiver versus a Conventional Tide Gauge', *Journal of Atmospheric and Oceanic Technology*, 34(2), pp. 295–307. Available at: https://doi.org/10.1175/JTECH-D-16-0101.1.

Löfgren, J. S., and R. Haas (2014) 'Sea level measurements using multi-frequency GPS and GLONASS observations', *EURASIP J. Adv. Signal Process.*, 2014, 50. Available at: https://doi.org/10.1186/1687-6180-2014-50.

Míguez, B.M., Testut, L. and Wöppelmann, G. (2012) 'Performance of modern tide gauges: towards mm-level accuracy', *Scientia Marina*, 76(S1), pp. 221–228. Available at: https://doi.org/10.3989/scimar.03618.18A.

Merrifield, M. (2010) 'The Global Sea Level Observing System (GLOSS)', in *Proceedings of OceanObs'09: Sustained Ocean Observations and Information for Society*. *OceanObs'09: Sustained Ocean Observations and Information for Society*, European Space Agency, pp. 695–701. Available at: https://doi.org/10.5270/OceanObs09.cwp.63.

Miguez, B.M., Gomez, B.P. and Fanjul, E.A. (2005) 'The ESEAS-RI Sea Level Test Station: Reliability and Accuracy of Different Tide Gauges'.

Miguez, B.M., Testut, L. and Wöppelmann, G. (2008) 'The Van de Casteele Test Revisited: An Efficient Approach to Tide Gauge Error Characterization', *Journal of Atmospheric and Oceanic Technology*, 25(7), pp. 1238–1244. Available at: https://doi.org/10.1175/2007JTECHO554.1.

NIVMER mission reports available online on LEGOS/ROSAME site at http://www.legos.obs-mip.fr/en/observations/rosame/communication/rapports/

Pérez, B., Payo, A., López, D., Woodworth, P.L. and Alvarez Fanjul, E. (2014) 'Overlapping sea level time series measured using different technologies: an example from the REDMAR Spanish network', *Natural Hazards and Earth System Sciences*, 14(3), pp. 589–610. Available at: https://doi.org/10.5194/nhess-14-589-2014.

Ponte, R.M. (2006) 'Low-Frequency Sea Level Variability and the Inverted Barometer Effect', *Journal of Atmospheric and Oceanic Technology*, 23(4), pp. 619–629. Available at: https://doi.org/10.1175/JTECH1864.1.

Pugh, D. (1987) Tides, Surges and Mean Sea Level: A Handbook for Engineers and Scientists. John Wiley & Sons, Chichester, 472 p.

Richter, A., Marcos, M., Monserrat, S., Gomis, D., Ruiz, S., Liebsch, G. and Dietrich, R. (2005) 'Comparison and Combination of Coastal and Off-Shore Tide Gauge Measurements from Eivissa Island, Western Mediterranean', *Marine Geodesy*, 28(4), pp. 271–289. Available at: https://doi.org/10.1080/01490410500411711.

Testut, L., Wöppelmann, G., Simon, B. and Téchiné, P. (2006a) 'The sea level at Port-aux-Français, Kerguelen Island, from 1949 to the present', *Ocean Dynamics*, 56(5–6), pp. 464–472. Available at: https://doi.org/10.1007/s10236-005-0056-8.

Testut, L., Wöppelmann, G., Simon, B. and Téchiné, P. (2006b) 'The sea level at Port-aux-Français, Kerguelen Island, from 1949 to the present', *Ocean Dynamics*, 56(5–6), pp. 464–472. Available at: https://doi.org/10.1007/s10236-005-0056-8.

Watson, C. S., R. Coleman, and R. Handsworth (2008), Coastal tide gauge calibration: A case study at Macquarie Island using GPS buoy techniques, *J. Coastal Res.*, 24(4), 1071– 1079, Available at: https://doi.org/10.2112/07-0844.1

White, L.B. and Boashash, B. (1990) 'Cross spectral analysis of nonstationary processes', *IEEE Transactions on Information Theory*, 36(4), pp. 830–835. Available at: https://doi.org/10.1109/18.53742.

Williams, S.D.P., Bell, P.S., McCann, D.L., Cooke, R. and Sams, C. (2020) 'Demonstrating the Potential of Low-Cost GPS Units for the Remote Measurement of Tides and Water Levels Using Interferometric Reflectometry', *Journal of Atmospheric and Oceanic Technology*, 37(10), pp. 1925–1935. Available at: https://doi.org/10.1175/JTECH-D-20-0063.1.

Woodworth, P.L. and Player R. (2003) 'The permanent service for the sea level: An update to the 21th century', J. of Coastal Rsearch,19, pp.287-295.

Woodworth, P.L. and Smith, D.E. (2003) 'A One Year Comparison of Radar and Bubbler Tide Gauges at Liverpool', *INTERNATIONAL HYDROGRAPHIC REVIEW*.

7 Appendix

Appendix A: Optical Levelling

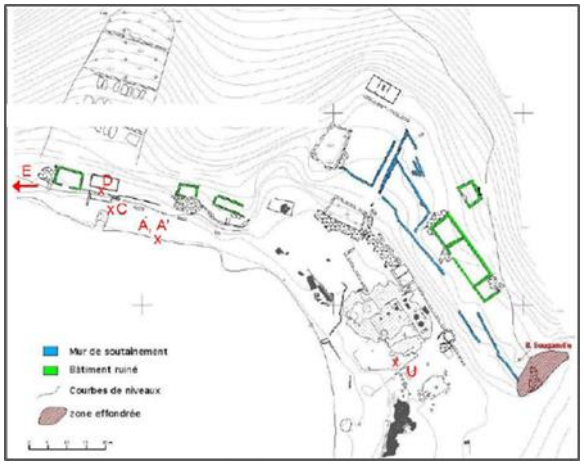

Figure A1: geodetic points levelled during the 2007-campaign (ref. Nivmer report)

- D: main marker sealed on the step-in front of the cabin,
- A and A': top of the ancient and new stilling tube corresponding now to the sensor mark I (upper plate of the tide gauge tube serving as a support for the SPA1 radar sensor)
- C: intermediate marker sealed in the rocks at the pier
- U intermediate marker sealed on concrete of old building
- E: the historical 1874 mean sea level mark

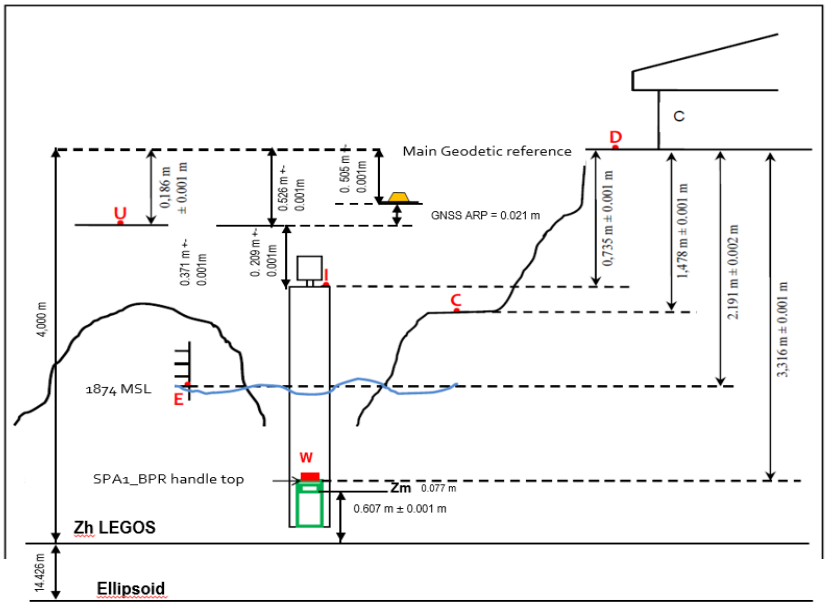

Figure A2: Summary of the levelling campaigns from 2007 and 2014. The leveling height of the geodetic benchmarks in referred to the Nivmer levelling campaigns of 2007, 2008, 2009. One-centimetre discrepancy exists with the levelling campaign from Mission Patrimoine in 2O10 for the benchmarks C and E. (Adapted from Nivmer report)

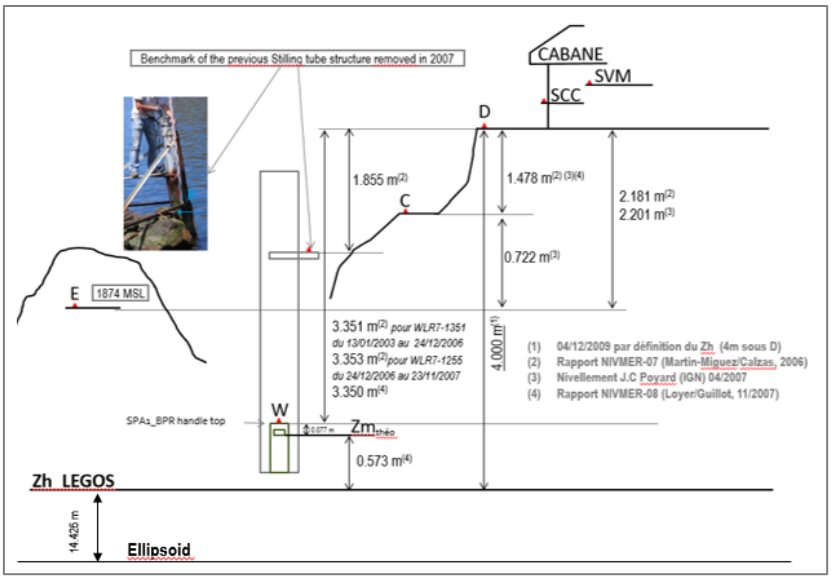

Figure A2: Summary of the levelling campaigns from 1994 to 2007 with the previous stilling tube ((Adapted from Nivmer report).

Appendix B: Typical Van de Casteele plots for instrumental error detection

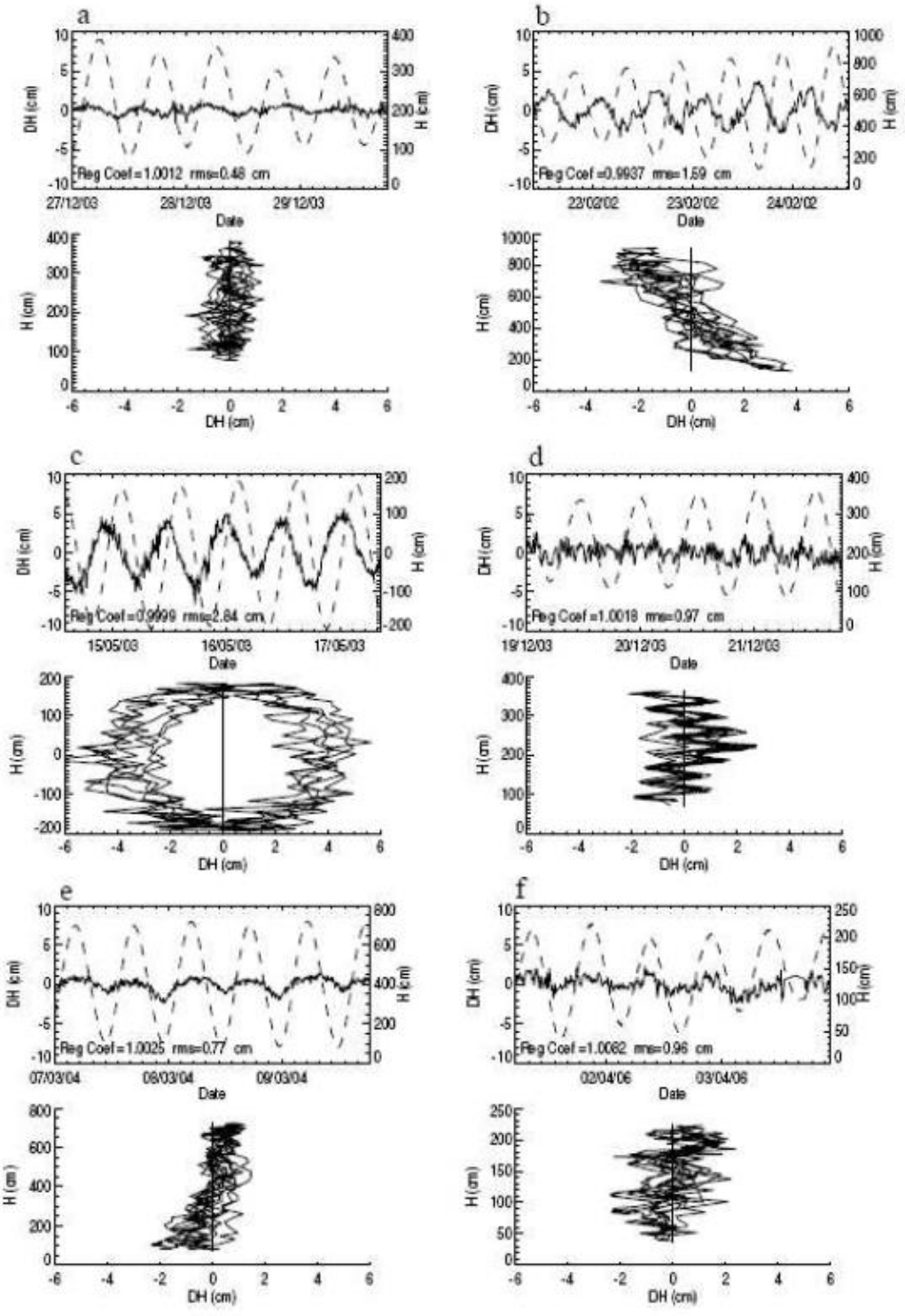

(source: Miguez et al., 2008)